Understanding and Controlling Rotation at the Single-Molecule Level

A dissertation submitted by

Heather L. Tierney

In partial fulfillment of requirements

for the degree of

Doctor of Philosophy in Chemistry

Tufts University

February 2011

Adviser: Prof. E. Charles H. Sykes

Abstract

As technology goes to smaller and smaller dimensions, efficient parts are needed on the same size scale in order to create nano- and micro-machines. Just as motors are needed on the macroscale to run engines, motors are needed in these tiny machines in order to convert a fuel source into productive work. While scientists have had trouble creating synthetic nano- and micro-scale motors, these sorts of "machines" are prevalent throughout biology. This thesis describes studies into the fundamental properties of rotating thioether molecules. Symmetric thioethers have been studied in detail as a function of chain length to clarify the similarities between the rotational barriers for thioethers with two or more carbons in each alkyl tail. Molecules were electrically-driven using pulses from the STM tip, and the mechanism for this rotation was elucidated. Using theoretical methods both the adsorption site and rotational pathway were revealed. Asymmetric thioethers were studied using both experimental and theoretical methods. Adsorption site dependent rotational properties were found, and the barrier to rotation was calculated to have an asymmetric torsional potential. It was discovered that due to the intrinsic chirality of even bare metal STM tips, that directed rotation could be achieved in the electrically-induced motion of surface-bound enantiomers. This directed motion shows for the first time that an electrically-driven rotary motor can be made from a single molecule.

Table of Contents

Understanding and Controlling Rotation at the Single-Molecule Level

Chapter 1

Introduction

Molecular machines driven by chemical, light or thermal energies are pervasive in nature;[1-4] however, little progress has been made toward creating synthetic counterparts. Molecular rotors and motors are crucial parts of many biological processes including cellular transport, cell division, muscle contraction, genetic transcription and translation.[1-3,5,6] The gap between nature and nanotechnology remains due to the limited fundamental understanding of the transfer of energy to mechanical motion at the nanoscale.[2,4]

Some impressive advances on ensembles of large organic molecules can be found in the literature studying rotors in the aqueous phase;[6-10] however, many potential applications of molecular rotors in nanotechnology would require their association with surfaces.[11-19] It is much easier to monitor and control surface-bound molecular rotors, and they can also be coupled with other nanomechanical devices. Surface-mounted rotations of small molecules, such as PF_3[20] and O_2,[21] as well as large organic molecules[11,13-15,22] have been reported. A

lot of attention has also been devoted to investigating rotational dynamics of porphyrins.[16-19,23-25] Using scanning tunneling microscopy (STM) rotational rates and energy barriers have been determined. A related technique of inelastic electron tunneling (IET) has been used to probe rotations of acetylene[21,26,27] and *cis*-2-butene molecules.[28,29] Rotational dynamics of chloromethyl- and dichloromethylsylil molecules on fused silica surfaces have been analyzed via STM and by measuring dielectric responses.[30-33] Experiments also show that halogenated thiophenol molecules can rotate on Cu{111} surfaces even at low temperatures.[34,35] Even a simple methane thiol (MeSH) molecule was observed to rotate on a Au surface with the S-Au bond as its axle.[36]

Surface properties of symmetric dialkyl sulfides (a.k.a. thioethers) have been investigated previously by our group and others.[37-43] Self-assembled monolayers (SAMs) of thioethers have been studied and compared to thiol-based SAMs.[39-43] While dialkyl sulfides have received much less attention than alkane thiols[44-49], they have nevertheless found multiple uses in applications ranging from materials and nanoparticle synthesis to self-assembly and surface modification. The dialkyl sulfide functionality has been utilized as a mediator for nanoparticle growth[50], a linker for nanoparticle assembly[50,51], a ligand for novel inorganic complexes[52], and as a way to tether a variety of functionalities to surfaces.[43,53] Small thioethers have also been shown to act as single molecule rotors and provide an excellent test bed for studying many aspects of molecular

rotation. The rotational properties of symmetric dialkyl sulfides have been studied as a function of chain length, temperature, and proximity to neighboring molecules.[37]

This thesis describes studies into the fundamental properties of rotating thioether molecules. Symmetric thioethers have been studied in further detail as a function of chain length in order to elucidate the similarities between rotational barriers for thioethers with two or more carbons in each alkyl tail. Molecules were electrically-driven using pulses from the STM tip, and the mechanism for this rotation was revealed. Using theoretical methods both the adsorption site and rotational pathway were revealed. Asymmetric thioethers were studied using both experimental and theoretical methods. Adsorption site dependent rotational properties were found, and the barrier to rotation was calculated to have an asymmetric torsional potential. It was found that due to the intrinsic chirality of even bare metal STM tips, that directed rotation could be achieved in the electrically-induced motion of surface-bound enantiomers. This work describes the first report of an electrically-driven single-molecule rotary motor.

1.1 Methodology

1.1.1 Experimental Methods: Scanning Tunneling Microscopy

Nearly 30 years after the scanning tunneling microscope (STM) was invented in 1981, its vast utility has continued to prevail in nearly every aspect of surface science. This instrument, which has often been said to have opened the door to nanoscience, allowed visualization of molecules, atoms and particles with a resolution that had never before been achieved. All rotor experiments described here were performed in a low-temperature, ultrahigh-vacuum (LT-UHV) scanning tunneling microscope (Omicron).[54] The very high stability of the microscope at 78 and 5-7 K allows for the study of a particular area of the surface for many hours, and point spectroscopy can be performed with a minimum amount of z-drift. The STM stage was equipped with a sample heater capable of controllably heating the sample and tip up to 40 K above the base temperature (of 5-7 K). Cu{111} and Au{111} single crystals were purchased from MaTecK and cleaned by cycles of argon ion sputtering (1 keV/14 μA) and annealing at 1000 K. After the final anneal, the crystal was transferred in less than 5 min into vacuum ($<5 \times 10^{-10}$ mbar) in the precooled chamber. In approximately 30 min, the sample cooled from room temperature to either 78 or 5-7 K. All images were recorded with etched W or cut Pt/Ir tips, and voltages refer to the sample bias. Molecular dosing and other specific procedures are described on a chapter-by-chapter basis, if not within the following sections of methodology.

1.1.2 Theoretical Methods: Density Functional Theory

Theoretical calculations were performed using for density functional theory (DFT). The Vienna Ab initio Simulation Package (VASP) was employed with ultra-soft pseudopotentials (USPP). All calculations used the Perdew and Wang (PW91) generalized gradient approximations (GGA) to describe the exchange correlation potentials. Specifics of surface slabs, geometry optimizations and other calculations are described within the relevant chapters.

1.2 Current vs. Time Curves

With STM it is possible to measure rotational events of the thioether molecules. If the STM tip is placed to the side of one of the molecule's lobes, all six positions of the rotating tails with respect to the underlying surface can be distinguished. In this measurement the feedback loop (which is normally used to modulate the STM tip height in order to maintain a constant tunneling current) is turned off and the tunneling current is monitored with respect to time (*I* vs. *t*). The current states that are measured are a reflection of the proximity of an alkyl tail of the rotor molecule to the STM tip (the closer the tail, the higher the tunneling current).

When taking *I* vs. *t* curves the position of the STM tip is very important. If the tip is placed off to the side of the rotating alkyl arms while the feedback loop is turned off, then the current measured by the fixed STM tip is proportional to

the distance between the tip and an alkyl tail. If the tip is placed too close to the center of the molecule, then it is no longer possible to differentiate between the positions of the alkyl tails. By placing the tip directly on top of a lobe of the alkyl tail, the next closest positions of the alkyl tail on either side of the tip would be equivalent. If the tip is placed asymmetrically off to the side of one of the alkyl tails, this breaks the degeneracy of current states farther from the tip. By measuring rotational events in *I* vs. *t* curves, it is possible to measure the rotational rate, which is simply the number of switching events per unit time. Since the current states are related to the positions of the alkyl tails relative to the tip, it is also possible to measure the directionality of the rotating molecule by following the progression of these current states.

The choice of conditions for *I* vs. *t* curves is also important. By plotting switching rate vs. tunneling current it is possible to discern the number of electrons used in the rotational process. A linear curve indicates a one electron process, a two electron process produces a parabola, etc. Alternatively, the natural log of the rate vs. the natural log of the tunneling current can be plotted; in which case, the slope of the line is the number of electrons in the process. When choosing voltage used for the curves, both high and very low voltages can lead to higher switching rates. Very low voltages cause the tip to move very close to the molecule being interrogated, which can form a partial bond between the molecule and the tip. This causes the molecule to be pulled off the surface

slightly, causing a lower barrier to rotation and a higher rotational rate. On the other hand, as the voltage is increased to higher tunneling voltages, then higher energy electrons are injected into the molecule. These electrons can excite rotation above a certain threshold voltage, which can be found by plotting switching rate vs. electron energy. Another condition which needs to be set for the rate vs. time curves is the raster time, which is the amount of time used to collect each point in the *I* vs. *t* curve. Raster time should be chosen carefully, so that it is sufficiently long in order to minimize the signal noise ratio in the curve enabling differentiation of subtly different current states. On the other hand, if the raster time is too long, then it is possible to miss events. Finally, the number of points per *I* vs. *t* curve should be chosen. It is possible to choose any number of points allowed by the scanning software; however, due to thermal drift while the feedback loop is off, it is not realistic to take extremely long curves because measurements at the beginning or end of the curve may be different. Instead, a shorter number of points (1000 to 10000) would be chosen, and the tip would be repositioned between each of a number of shorter curves. Measurements for rate data would be collected and averaged for a single molecule at a time, not a population of molecules in order to minimize effects due to variations between different molecules.

1.3 Automated Counting Program

In order to cut down on the analysis time for counting switching curves, an automated program was created with the help of the University Information Technology (UIT) department. This program was developed in order to calculate the number of rotational events within a *I* vs. *t* curve based on the user-defined ranges of tunneling currents for each rotational state. For each switching curve the user would need to examine the curve and designate the current ranges for each rotational position. Then, the counting program would assess each point within the *I* vs. *t* curve in order to assign the molecule's position based on its designated current range. If a point did not fit into one of the pre-assigned ranges, it was excluded and discounted for switching measurements. Based on the progression of points within the data set, the program would assign switching events when the current range changed between two points. The program ignored excluded points, and did not count consecutive points within the same state.

This counting program unfortunately suffered from intolerable problems. Any slight amount of thermal drift in the system (which is almost impossible to completely negate) tilted the baseline of the *I* vs. *t* curve. This slight slant in the curve meant that a current state may shift in range from the beginning to the end of the curve. As low current states are very close together, this means that it is very difficult to assign appropriate ranges that work for the entire curve. It also

means that even the slightest bit of noise in the measurement often gets interpreted as switching events. Due to these factors, the automated counting program was not used for quantitative measurements, as it would only provide an approximate, relative switching rate. Curves had to be counted by hand, where the user would determine switching events by examining the *I* vs. *t* curves one by one.

1.4 Height Measurements for Chiral Molecules

In order to measure the heights for populations of molecules, careful measurements were made using line scans. Images needed to be sufficiently flattened, but without the use of any form of line correction in order to provide the accurate height of each molecule. These line scans needed to be long enough to reach the full minima of the surface between the molecules. The lines were stretched across two opposing lobes in a molecule and the line was moved perpendicular to these lobes until the maximum height across the molecule was found. The height was then measured as the difference between this maxima on the molecule and the surface minima within the same line. Exceptions were made when locating the maxima on the molecule if a saturated point was found (which could be easily spotted as not being within the natural curve of the molecular shape). Height differences were averaged for a collection of molecules

within a tip state, over many areas of the surface while making sure that a constant tip state was maintained.

Chapter 2

Dynamics of Thioether Molecular Rotors: Effects of Surface Interactions and Chain Flexibility

2.1 Introduction

Experimental achievements in the development and analysis of molecular rotor systems have stimulated theoretical efforts to understand rotational dynamics.[22,36,55,56] Michl and Horinek[55,56] investigated altitudinal molecular rotors using Molecular Dynamics (MD) computer simulations based on the universal force field (UFF) and taking into account electronic friction on the surface. Theoretical computations have suggested that there are several dynamic regimes of rotation. A different approach has been applied in Refs.[22,36] where rotational barriers have been calculated by utilizing quantum-chemical density-functional methods. Although theoretical studies have helped to explain some of the experimental observations, they were not able to explain the mechanisms of rotational dynamics on surfaces.

Our group has used a new stable and robust system of molecular rotors, which consists of thioether molecules bound to gold surfaces, to study rotational properties of small molecules.[37] In this system the molecular rotation could be stimulated either thermally or mechanically. STM has been used to obtain the

rotational properties of thioether molecules at different temperatures. Experiments have shown that dimethyl sulfide has a low activation energy for its rotation, while all other investigated dialkyl sulfides (with longer chains) have similar rotational barriers. This result was rather surprising since one could argue that longer alkyl chains should interact stronger with gold surface, significantly slowing down the rotations of individual molecules. In this paper, mechanisms for the rotation of thioethers on Au have been investigated by utilizing a comprehensive approach that combines both experimental and theoretical methods.

2.2 Experimental Methods

Thioethers (between 99.9 and 99.95% purity) were obtained from Sigma Aldrich and were further purified by cycles of freeze/pump/thaw prior to introduction to the STM chamber via a leak valve. The molecules were deposited onto the sample by a collimated molecular doser while the tip was scanning. The STM stage was equipped with a sample heater capable of controllably heating the sample and tip up to 40 K above the base temperature.

2.3 Theoretical Methods

To understand the mechanisms of molecular rotation for thioethers on gold surfaces Molecular Dynamics computer simulations were performed which

utilized a recently developed method for the analysis of thermally-induced motions of nanocar molecules.[57] This method is based on rigid-body MD calculations that utilize the universal force field (UFF). The advantage of this approach for analyzing the rotational dynamics of thioethers is that almost all atomic interactions are explicitly taken into account while some of the internal degrees of freedom are neglected. This allows the calculations to be sped up significantly, yielding longer trajectories and providing a better description of dynamic properties.[57]

2.3.1 Calculation Details

Rigid-body MD calculations were performed in order to study the rotational dynamics of a series of symmetric dialkyl sulfides ($CH_3(CH_2)_n$-S-$(CH_2)_nCH_3$) with n = 0,1,2,3. For simplicity, these molecules were labeled as C_n+1, which corresponds to the number of carbon atoms in each alkyl chain. Before simulations were performed, all initial structures were optimized such that they were always started from states close to equilibrium. For each molecule and each of the five temperatures used (25, 35, 50, 78 and 100 K), ten trajectories were obtained. To maintain a constant temperature in the simulations, a Nose-Poincare thermostat[58] with the symplectic integrator for rigid-body MD was utilized.[59] All trajectories were 2.5-5 ns long since a variable time-step approach was used. The UFF force field[60] was employed to describe intra-molecular

interactions in thioethers and some interactions between the surface and the molecules under consideration. To describe chemisorption of the sulfur atom, a Morse-type binding term was chosen. All parameters for the intra-molecular interactions were calculated on the basis of the UFF force field rules. The parameters of the Morse-type binding functional were adopted from different sources,[60,61] and were subject to variation.

The surface potential was constructed in the following way. For each atom in the thioether molecule its coordinates were projected onto the surface plane and a lattice cell was reconstructed around the projection of the atoms in the thioether. This cell was represented by 4 explicit atoms in a fcc(111) coordination (parallelogram). The rest of the surface potential was modeled by constructing the explicit surface potential via replicas of this minimal lattice cell. Usually N=5 lattice cells were used on each side of the initial central cell around the projection. The size of the surface slab was $b(2N+1)$ = 31.66Å, where b is the lattice size of the (111) surface. Bonded surface-molecule interactions have been also modeled explicitly. The same projection approach has been used for bonded surface-molecule interactions, but with Morse potentials instead of Lennard-Jones potentials. To avoid discontinuity in the potential that could lead to anomalous diffusive behavior and could bias results, the following switching function was used:

$$SW\left(R, R_{on}, R_{off}\right) = \begin{cases} 1, R < R_{on} \\ \left(\frac{R_{off} - R}{R_{off} - R_{on}}\right)^3 \left[1 + 3\left(\frac{R - R_{on}}{R_{off} - R_{on}}\right) + 6\left(\frac{R - R_{on}}{R_{off} - R_{on}}\right)^2\right], R_{on} \le R \le R_{off} \\ 0. R > R_{off} \end{cases} . \quad (1)$$

Parameters for the switching function were chosen to be $R_{on} = 2\sqrt{3}b$ and $R_{off} = 5b$, where $b = \frac{a}{\sqrt{2}}$ and is the lattice size of (111) surfaces. In addition, charges for each molecule were computed before each simulation using a charge equilibration scheme for molecular dynamics.[60]

In the experimental studies a Au(111) surface was used, which reconstructs into three different domains. Since the properties of the surface could be critical for rotational dynamics, MD simulations for C1-C6 molecular rotors (except C5) were also performed on three different domains of the reconstructed gold surface. The gold surface was represented by three layers with a total number of atoms around 1150. In order to obey the periodicity of the reconstructed surface at least eleven shells (unit cells) had to be used in the direction of reconstruction, but typically sixteen shells were used to avoid discontinuities in the potential. Thus the size of the super-lattice unit was 2.88 Å *22 = 31.68 Å in the reconstruction direction and 2.88 Å in the perpendicular direction. The first layer was different, as it was contracted in one of the directions (the reconstructed direction) by a factor of (22/23).

Three different surface sites were considered, which corresponded to fcc, hcp and sol (soliton) domains. The center of the molecule was placed on each of these areas and then the energy was minimized. Simulations were performed starting in these three different areas and while some molecules diffused around the surface during simulations (especially at high temperatures), in most cases (especially at low temperatures) molecules were mostly immobile.

2.3.2 Analysis of the MD Trajectories

In the STM experiments the rotational frequency of the molecules was measured by recording the switching events between three distinct orientations. Each orientation was associated with some average state of the tunneling current, and the rotational rate was measured as a frequency of changing between these orientations. In our simulations a similar analysis has been done.

A vector,

$$\vec{R}_{21} = \vec{R}\left(C_{\alpha,left}\right) - \vec{R}\left(C_{\alpha,right}\right), \qquad (2)$$

was chosen to connect two α-carbons in each chain as a vector that determines the time-dependent orientation of the molecule. This angle, $\phi(t)$, was then defined as the angle between this time–dependent vector and some predefined fixed direction. This angle was assumed to be a variable describing the orientation of the molecule with respect to the surface. Since the angle is a

continuous function, a threshold value for ϕ was also introduced to distinguish between the three discrete states, as was done experimentally.

2.4 Results and Discussion

Using low-temperature scanning tunneling microscopy (STM), individual thioether molecules could be imaged as hexagons at 78 K (see Figure 2.1). As the molecules rotated with the Au-S bond as their axle, the rotors spent most of their time in three orientations due to the three-fold symmetry of the underlying Au{111} substrate. In Figure 2.1a six lobes are clearly visible due to these three nearly equivalent orientations. If the lobes of the thioethers were labeled as the head or the tail, there are actually six possible orientations with respect to the surface, although only three states are distinguishable due to the symmetry of this molecule. Further imaging with atomic resolution (Figure 2.1b) shows the Au atoms resolved over the rotor, allowing the adsorption site of dibutyl sulfide (C_4) to be estimated as near three-fold.

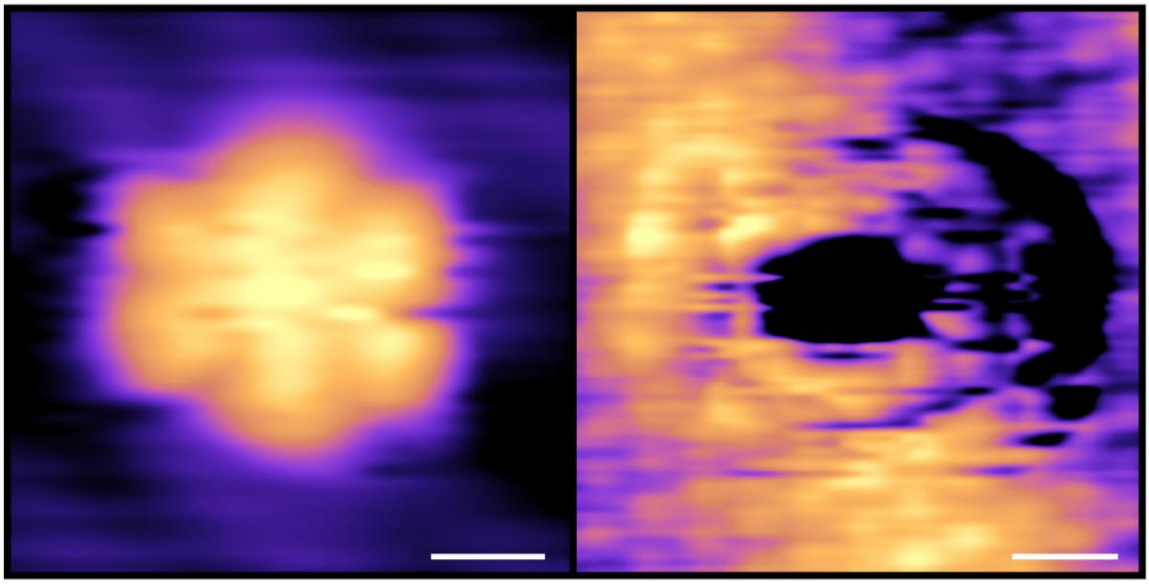

Figure 2.1: STM images of dibutyl sulfide (C4) hexagons. (a) C4 images as a hexagon with six distinct lobes due to its three nearly equivalent orientations with respect to the underlying Au lattice (I = 0.1 nA, Vtip = 0.3 V, 7 K). (b) Atomic resolution of the Au substrate resolved over a C4 molecule helps estimate the adsorption site (I = 0.5 nA, Vtip = -0.2 V, 78 K). Scale bars = 0.5 nm.

At 7 K, all of the thioether molecules imaged as mostly linear, with the exception of dimethyl sulfide (C_1), which already appeared hexagonal due to its low barrier to rotation. As the thioethers were heated, they began to spin and quickly became hexagonal. For diethyl (C_2), dibutyl (C_4) and dihexyl (C_6) sulfide, the rotors appeared hexagonal at approximately the same temperature of 16 ± 2 K (see Figure 2.2). C_6 never imaged exceptionally well, probably due to the extra degrees of freedom from the length of the alkyl chains, but it too looked roughly hexagonal at 16 K.

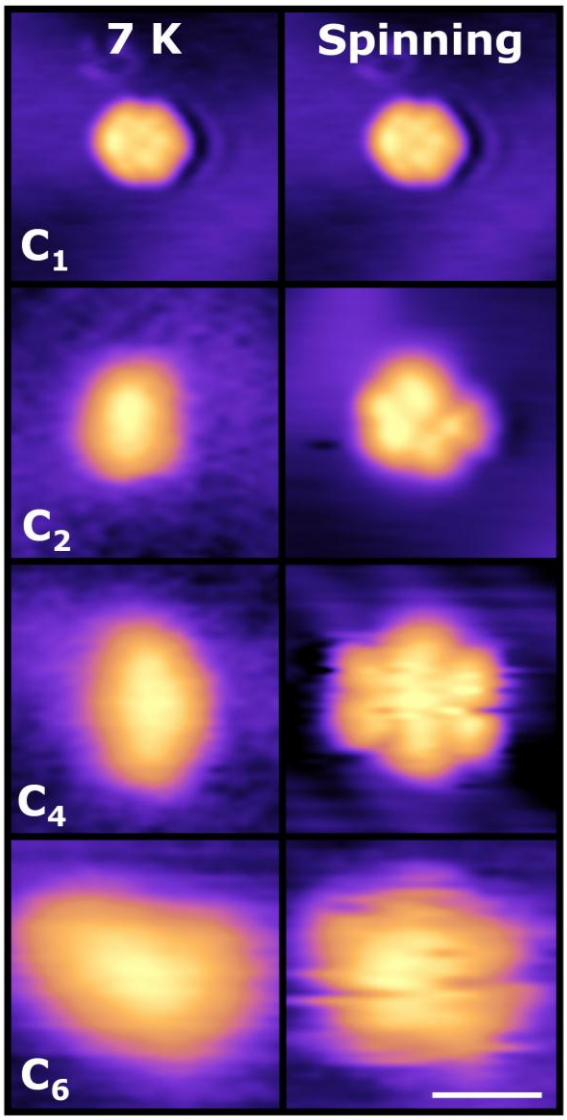

Figure 2.2: Dialkyl sulfide molecules are seen to spin at higher temperatures. Dimethyl (C_1), diethyl (C_2), dibutyl (C_4) and dihexyl (C_6) sulfide molecules are shown as linear vs. hexagonal molecules with the exception of C_1. C_1 has a low barrier to rotation, so it is seen to be spinning already at 7 K. Scale bar = 1 nm.

MD simulations provided trajectories for the motion of individual molecules from which the rotational dynamics of the thioethers could be analyzed. As shown in Figure 2.3, temperature strongly affected rotation. Similar to experimental observations, at low temperatures C_1 molecules already rotated

quickly, while C_4 rotated very slowly (Figure 2.3a). This observation could be deduced from the fact that C_1 occupied all six possible orientations with almost equal probability (corresponding to the six lobes imaged in STM); however C_4 preferred only one configuration during the time of one MD simulation. This situation changed at higher temperatures (Figure 2.3b) where C_4 also started to rotate faster due to a decrease in the effective rotational barriers.

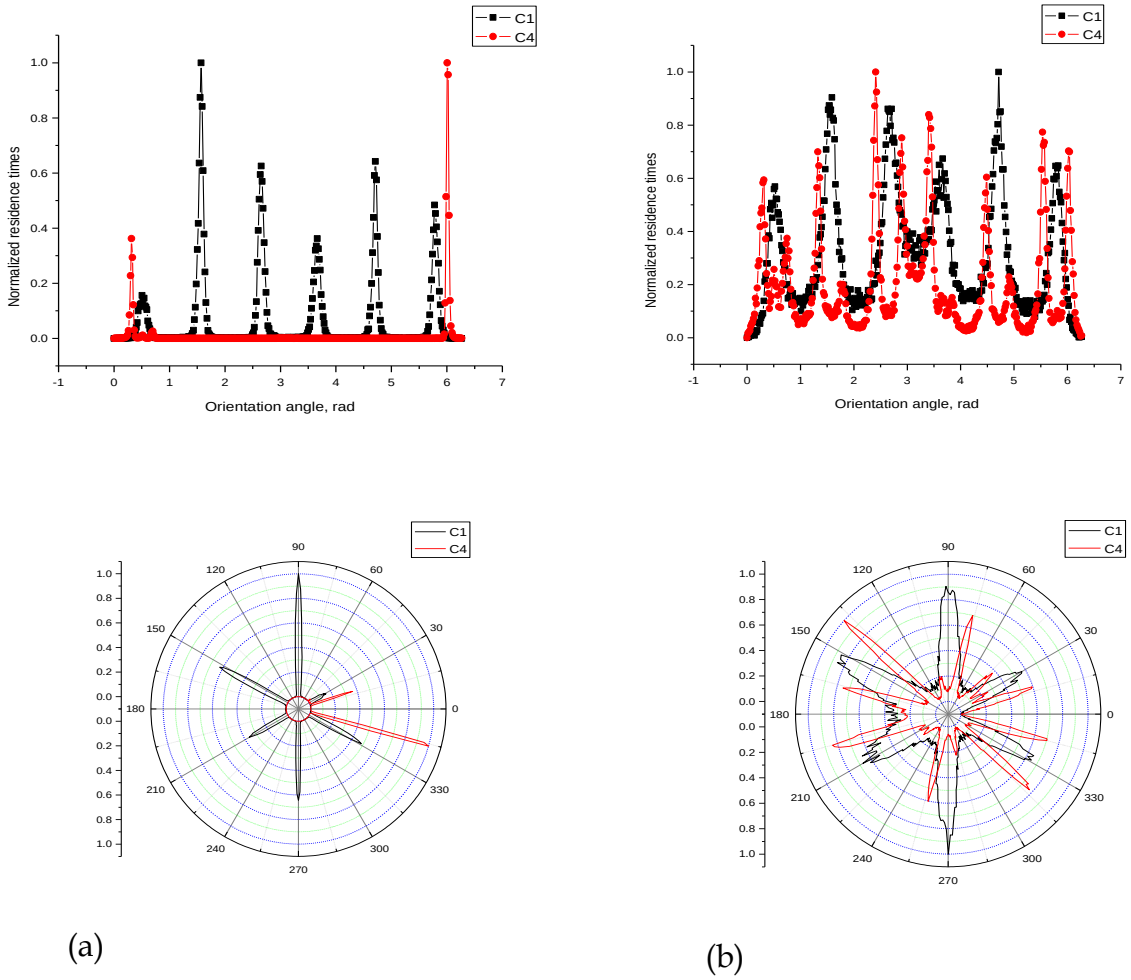

Figure 2.3: Temperature dependence of rotation dynamics of thioethers. Linear and polar plots are shown for the distributions of orientation angles for C1 and C4 molecules. (a) T=25 K. (b) T=100K.

Due to the compression of the Au(111) surface, an intermediate state between the linear and hexagonal molecules could be seen upon heating the thioethers. Since the Au substrate is compressed in one direction (leading to the characteristic herringbone reconstruction), the three-fold symmetry is broken slightly. This causes one of the three nearly-equivalent orientations of the molecule to lie at a slightly different energy than the other two. This small difference in energy causes the thioether molecules to appear rectangular before they spin fully and image as hexagons (see Figure 2.4). This intermediate, rectangular state occurs for both diethyl (C_2) and dibutyl (C_4) sulfide molecules at 12 ± 3 K.

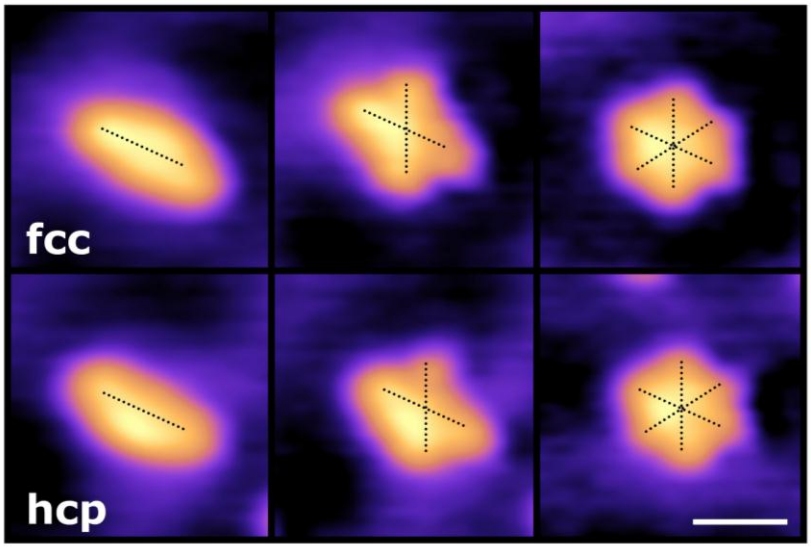

Figure 2.4: As dibutyl sulfide (C_4) molecules are heated, their appearance changes from linear to rectangular to hexagonal as the molecules sample two then three of the nearly equivalent orientations on the Au surface. (I = 10 pA, V_{tip} = 0.3 V. T_{linear}: 7 K, $T_{rectangular}$: 13 K, $T_{hexagonal}$: 25 K). Scale bar = 1 nm.

The details of how temperature affected the rotational efficiency of dibutyl sulfide (C_4) molecules are presented in Figure 2.5. At T=25K the C_4 molecule was preferentially found in only one orientation because it did not have enough energy to explore other potential minima in the free-energy profile. At T=78K the thermal energy was high enough to overcome some of the rotational barriers, and C_4 was found at four possible orientations with similar probabilities. At even higher temperature (T=100K) the number of preferred orientations increased to six. In addition, the rotational dynamics were similar on fcc and hcp surface domains. These theoretical results directly correspond to the linear, rectangular and hexagonal shapes seen in the STM images (see Figure 2.4).

It should be noted that the number of possible orientations is determined by the symmetry of the system. If only the first layer of the Au(111) surface is taken into account, then only six possible orientations of the molecule should be expected (assuming that one alkyl chain is the head and the other one is the tail). However, due to the presence of the second and the third layers, there are six additional orientations due to two separate types of three-fold site based on the Au atoms in the 2nd layer. For this system, one of these three-fold sites is less energetically favorable. In addition, MD runs are limited to several nanoseconds, limiting the possibilities for the exploration of thioethers on the surface. These are the main reasons why more complex orientation probabilities were observed with smaller peaks at higher temperatures, as shown in Figure 2.4.

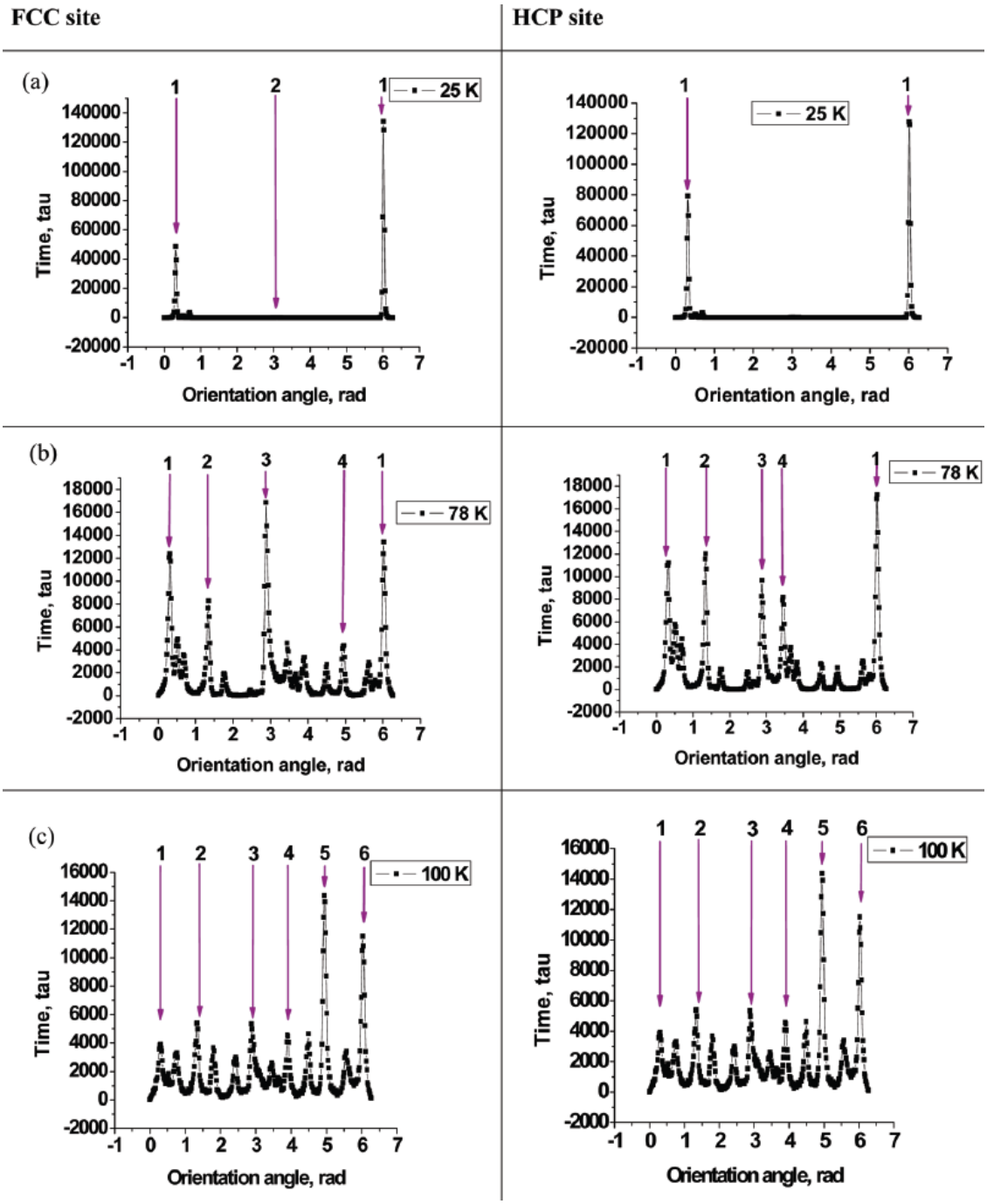

Figure 2.5: Rotational dynamics of dibutyl sulfide (C4) on fcc and hcp lattice sites at different temperatures. Plots are shown for the distributions of orientation angles. (a) T) 25 K; (b) T) 78 K; (c) T) 100 K.

Quantitative analysis of MD trajectories allowed the rotational frequencies of thioethers to be measured. The results for the rotational activation energies are presented in Figure 2.6. Similar to experimental observations, computer simulations predicted a jump in rotational barriers when going from C_1 to C_2 molecules, however the activation energies were almost constant or very slowly increased (although this depended on the surface domain). Experiments showed almost unhindered rotations of the C_1 molecules with a barrier of less than 0.5 kJ/mole,[37] while MD calculations gave an activation energy closer to 1 kJ/mole. For C_4 the agreement between the theory and experiments was better: STM measured the barrier at about 1.2 kJ/mole,[37] and theoretical computations yielded ~1.5 kJ/mole.

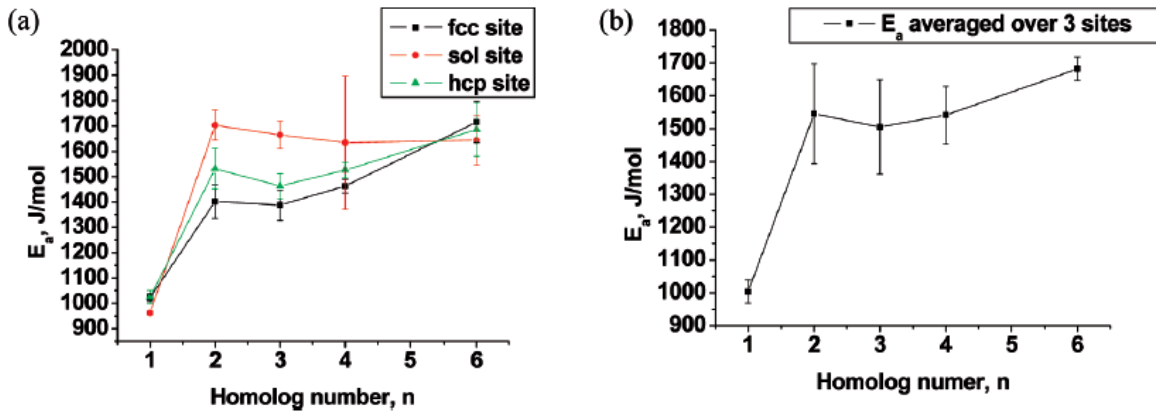

Figure 2.6: Activation energies for surface rotation of the thioethers as a function of the number of carbon atoms in alkyl chains. (a) Activation energies for three distinct surface sites: fcc, hcp, and soliton (sol). (b) Activation energies averaged over different surface sites.

The observation that rotational barriers were almost independent of the alkyl chain length for C_n molecules (for n larger than 2) is counterintuitive since one could argue that for larger side chains, the number of interactions with the gold surface increases and the rotational activation energies must be strongly increasing functions of n. These predicted trends were not observed experimentally. The alkyl side chains of the molecules were rather flexible and as a result, in most of their molecular conformations, only part of the molecule was exposed to the surface. Thus, there were two factors that defined the rotational activation energies. Increasing the length of the alkyl chain led to stronger interactions with the surface (due to the larger number of atoms interacting with the surface) and slowed down the molecular rotations. However, larger alkyl chains were more likely to fold, which decreased the number of atoms that interacted with the surface, and significantly lowered the activation barriers. It seems from experimental measurements and from MD computer simulations that these factors almost cancel each other out for larger C_n molecules.

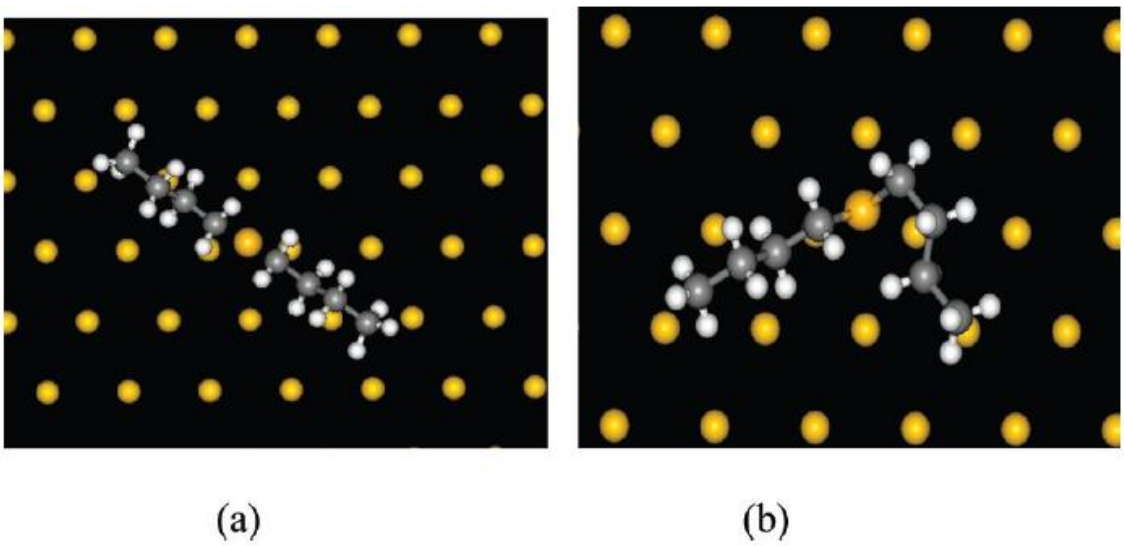

Figure 2.7: Structures of the dibutyl sulfide molecule (C4) with artificially frozen degrees of freedom. (a) Fully frozen, 1 linear rigid group; (b) Partially frozen, 3 rigid groups: 2 alkyl chains and a sulfur atom.

To test this idea, MD computer simulations were run for molecular rotors with some artificially constrained degrees of freedom. This theoretical method was based on the description of any molecule as a collection of coupled rigid-body segments, and the motion of these segments was generally independent of each other. In these MD calculations, the C_n molecules were viewed as consisting of (2n+1) rigid segments. To freeze some internal dynamics in the molecules, the number of rigid segments was decreased. For example, a fully frozen molecular rotor is made of a single linear rigid segment. Structures of fully frozen and partially frozen C_4 molecules are illustrated in Figure 2.7. The results for the rotational barriers of C_4 molecules with different internal degrees of freedom are presented in Table 2.1. Full freezing the molecular motion led to a significant increase in the activation energies, which was expected from the theoretical

calculations. However, partial freezing of alkyl chains did not change the rotational barrier very much. This can be understood if one imagined that the rigid alkyl chains in this artificial molecule were free to move around the sulfur atom in any direction. There were also many molecular conformations where the chains were not close to the gold surface, and this lowered the effective interaction. The rotational properties for different thioethers were also calculated with frozen degrees of freedom and then compared to the fully-flexible, realistic molecules. Figure 2.7 shows that molecules with frozen degrees of freedom should have rotated much slower. This observation supported the idea that folding dynamics of alkyl chains was responsible for lowering the effective rotational barriers in thioethers. These results also suggest the rotational dynamics of thioethers can be controlled and modified by changing the flexibility of the side chains.

TABLE 2.1: Activation Energies for Dibutyl Sulfide (Bu_2S) Molecules with Different Degrees of Allowed Internal Motions

type of freezing	activation energy (E_a) J/mol
fully flexible molecule = 9 rigid groups	1214.06
frozen alkyl chains = 3 rigid groups	1202.58
frozen molecule = 1 rigid group	2754.55

2.5 Conclusions

This study presented a comprehensive experimental and theoretical investigation of molecular rotations of symmetric thioethers on gold surfaces. Measuring rotational dynamics of single molecules at different temperatures using STM revealed that the activation barrier was almost constant for dialkyl sulfides with different alkyl chain lengths, with the exception of the smallest (dimethyl sulfide) which rotated significantly faster. These results seem to contradict the naïve expectations that increasing the number of atoms should increase the effective interactions with the surface and slow the rotational dynamics. To resolve the mechanism of the unusual rotational dynamics of thioethers rigid-body molecular dynamics simulations were performed. These theoretical calculations for the rotational properties of dialkyl sulfides were in good agreement with observed experimental properties. To explain this observed behavior a hypothesis was proposed that rotational dynamics is determined by two factors, the length of alkyl chains and the flexibility of the molecules. Because the side chains were flexible, the effective number of atoms that strongly interacted with the surface was rather small, and the rotations were not hindered significantly by increasing the length of the alkyl segments. MD simulations were also performed for molecular rotors with frozen folding dynamics, and these calculations showed a significant increase in the rotational barriers, which agreed with theoretical predictions.

These experimental and theoretical investigations show that this system using dialkyl sulfides on a gold surface is convenient and robust for studying rotors at a single-molecule level. To understand general mechanisms of rotational motion, it will be important in future works to investigate asymmetric rotors, dipolar rotors and molecules with different groups that strongly interact with the surface.

Chapter 3

Mode Selective Electrical Excitation of a Molecular Rotor

3.1 Introduction

Our work with thioether molecules bound to metal surfaces has offered a method with which to study the rotation of individual molecules as a function of temperature, molecular identity, proximity of neighboring molecules, and surface structure.[37,38,62] Arrhenius plots for the rotation of dibutyl sulfide yielded a rotational barrier of 1.2 ± 0.1 kJ/mol.[37] While these results revealed that small amounts of thermal energy are capable of inducing rotation, thermodynamics dictates that thermal energy alone cannot be used to perform useful work in the absence of a temperature gradient. Therefore, for molecules to meet their full potential as components in molecular machines, methods for coupling them to external sources of energy that selectively excite the desired motions must be devised.[21,29,30,63-68]

3.2 Experimental Methods

Dibutyl sulfide (99.95% purity) was obtained from Sigma Aldrich and further purified by cycles of freeze/pump/thaw prior to introduction to the STM

via a leak valve. The fully deuterated dibutyl sulfide was custom synthesized by Chemtos Custom Synthesis and its purity was verified by NMR to be >95%.

3.3 Results and Discussion

This paper describes a study of the electrical excitation of individual dibutyl sulfide (Bu_2S) molecular rotors with electrons from a scanning tunneling microscope tip. Action spectroscopy was used to measure the effect of electron energy on the rate of rotation.[21,29,66] The results revealed that tunneling electrons above a threshold energy excited a C-H vibration in the rotor's alkyl tail that coupled selectively to rotation of the whole molecule. Figure 3.1a shows an STM image of an individual Bu_2S molecular rotor on a Au{111} surface at 7 K. When imaging at 7 K under non-perturbative conditions (V = 0.3 V, I = 10 pA), the molecules were static and appeared in STM images as crescent-shaped protrusions. Figure 3.1b shows an image of a dibutyl sulfide molecule at 78 K, revealing that at this temperature the molecule rotated much faster than the timescale of imaging (~ 2 mins per image) and appeared as a hexagon due to fast interconversion between three distinct orientations that align with the high symmetry directions of the Au{111} surface.[35,36] The fact the rotating molecules always appear hexagonal over a wide temperature range (20-78 K) means that while the molecules can rotate very quickly ($1x10^6$ at 78 K)[2], they spend most of their time in the three distinct orientations on the surface. It was found that at

temperatures below 8 K the molecules were static and could be stably imaged for many hours at tunneling voltages less than ±0.35 V. However, either imaging or positioning the STM tip over the molecules at biases above ±0.35 V caused them to switch between their three distinct orientations. The white circles in images 3.1d and e mark the position at which 0.7 V tunneling electrons were delivered to a static molecule at 7 K and the corresponding *I* vs. *t* curve is shown in Figure 3.1c. It is clear from comparison of the two images (d & e) that the electrical excitation caused the molecule to rotate away from its starting point.

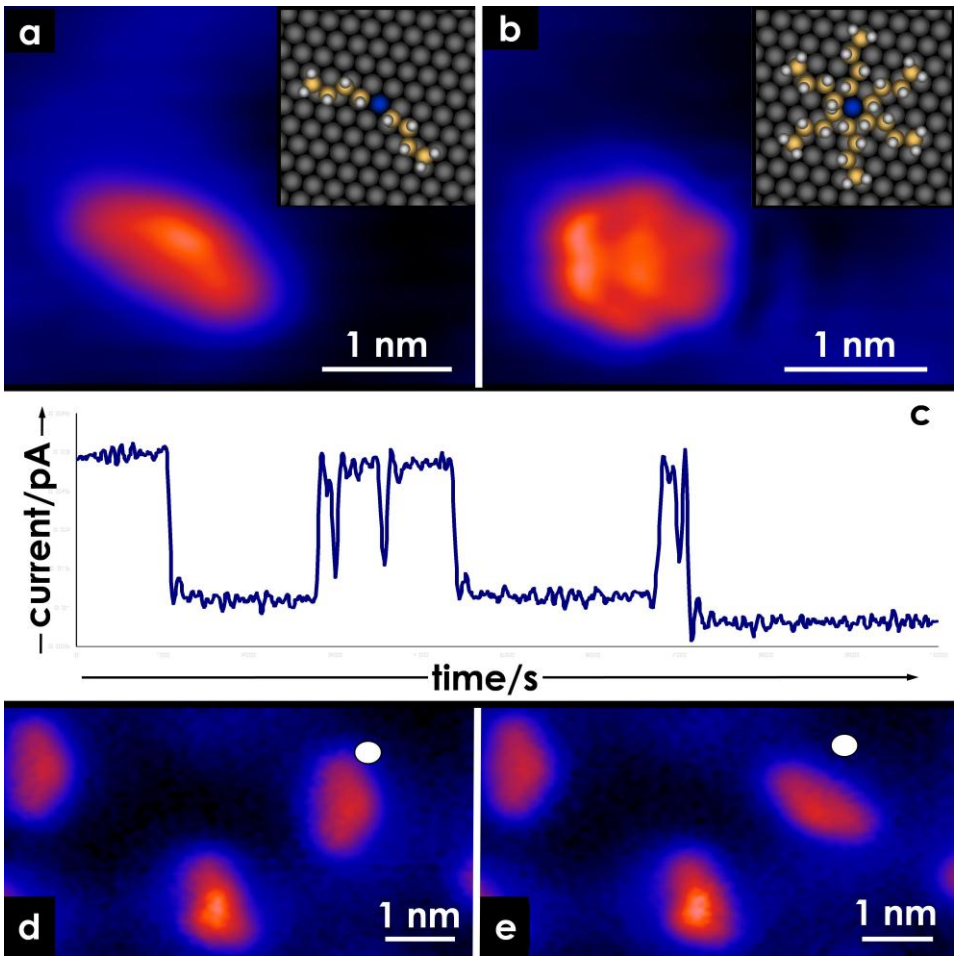

Figure 3.1: Panels a and b show STM images of static and spinning dibutyl sulfide molecular rotors on Au{111} at 7 and 78 K respectively. Schematics of the static and spinning rotors appear in insets. Panel c shows a tunneling current vs. time (I vs. t) curve taken during an electron-induced rotational excitation of the rotor seen in panel d. The white circles in d and e mark the electron injection point. Panel e shows that after excitation the molecule rotated to a new orientation. (Imaging conditions: a) 10 pA, 0.3 V, 7 K; b) 50 pA, 0.1 V, 78 K; d & e) 3 pA, 0.2 V, 7 K. Voltage pulse conditions: 3 pA, 0.7 V).

Close inspection of the *I* vs. *t* trace recorded during the 0.7 V pulse revealed that over the duration of the pulse, the molecule switched orientation several times before being re-imaged in its final position. Using this technique, individual molecules could be rotated simply by raising the tip voltage and monitoring the tunneling current until a change was observed, after which

imaging at a lower bias revealed that the molecule had indeed rotated to a new orientation. As the feedback loop (which adjusts the STM tip height to maintain a constant tunneling current) was turned off during the pulse, each reorientation of the molecule resulted in a different baseline tunneling current. Therefore, these changes in current could be equated with rotation of the molecule to a new orientation. In order to elucidate the mechanism of the electrical excitation, action spectroscopy was performed. This technique correlates the occurrence of a molecular event such as internal rearrangement, translation, dissociation or rotation to the energy of the electrons inducing the process.[21,29,63-68]

Figure 3.2a shows action spectra collected by placing the STM tip at the edge of a dibutyl sulfide molecular rotor with the feedback loop switched off such that the tip could both excite the molecule and monitor its rate of rotation by recording changes in the tunneling current. The rotation rate was measured as a function of sample bias at constant tunneling current and at temperatures <8 K so that minimal thermally-induced rotation occurred. It is clear from Figure 3.2a that a sharp increase in rotation occurs at energies above 360 meV. Derivatives of the fits of the data in Figure 3.2a revealed that this rotational onset energy of 375±5 meV was independent of the direction of the tunneling current. Such symmetric features are characteristic of inelastic electron excitation of a molecular vibration that is insensitive to the direction of electron flow. Onset energies of ~360 meV are characteristic of a C-H stretching mode excitation.[69-71]

The C-H stretch excitation energy has been probed using inelastic electron tunneling spectroscopy in a variety of surface bound molecules and measured at an energy of 358 meV for acetylene[71], 362 meV for trans-2-butene[70], and 395 meV for the HCC fragment of dehydrogenated acetylene[69].

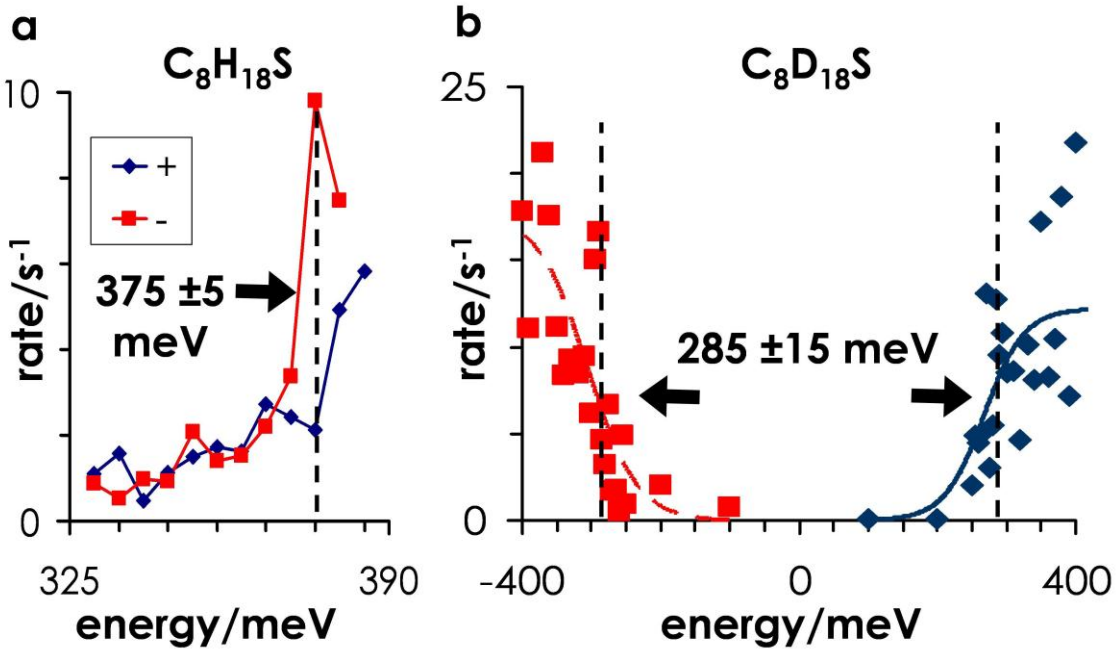

Figure 3.2: Action spectra (linear plot of rotation rate vs. tunneling electron energy) for both hydrogenated (a) and deuterated (b) dibutyl sulfide. The ~1/√2 shift for the deuterated version of the molecular rotor confirms the assignment of a mechanism involving inelastic electron excitation of a C-H(D) stretch that couples to rotation of the molecule. The bold arrows mark the onset energies. (Current: a) 5 pA, b) 150 pA).

In order to further verify that the mechanism involved inelastic electron tunneling excitation of a C-H stretch, a fully deuterated version of the molecule was custom synthesized. Similar isotope labeling experiments have shown shifts of ~1/√2 in the C-D stretch frequency. Measurements include 266 meV for d-

acetylene[71], 268 meV for d-trans-2-butene[70], and 313 meV for the DCC fragment of dehydrogenated d-acetylene[69]. Figure 3.2b shows that the corresponding onset voltage for the deuterated molecular rotor is shifted to the lower energy of 285±15 meV and that the onset is also symmetrical about zero.

Interestingly, in order to record action spectra for the deuterated molecular rotor, tunneling currents 30x higher were required to induce comparable rotation rates. It is well documented that the inelastic electron cross section for the C-D bond is ~30% lower than C-H[29,66,71,72], however, this small difference is insufficient to explain the 30x drop in the rotation rate of the deuterated rotor. In order for a high energy C-H (375 meV) stretch to couple to a low barrier rotation (1.2 kJ/mol = 12meV[37]) the energy must be redistributed into lower lying modes.[21,29,63-66] Previous experiments have shown that this energy transfer can occur via anharmonic coupling of high energy vibrational modes into lower energy rotational and frustrated translational modes.[21,29,63-66] It has even been demonstrated that molecular translation or desorption events can be selectively excited if the correct input energies are chosen.[65] These coupling efficiencies are dependant on both the type and the energy of all the vibrational and rotational modes of the molecule.[63,65,66] As dibutyl sulfide contains 27 atoms, the details of how the coupling occurs is beyond the level of current theory, but the fact that C-H stretches can drive rotation suggests that the rate of relaxation via energy transfer to the surface is not fast enough to completely quench the

observed rotation.[21,28,29,63,65-68] It is therefore not surprising given the complex transfer of energy through different modes of the molecule that dibutyl sulfide and its deuterated counterpart have different coupling efficiencies. Overall, excitation of dibutyl sulfide (at 400 meV) and its deuterated counterpart (at 300 meV) gave $1x10^{-6}$ and $5x10^{-8}$ rotations per electron respectively. To put these numbers in context, the Kawai and Ho groups have measured the rotational efficiencies of surface-bound butene and acetylene as $1x10^{-9}$ and $2x10^{-10}$ rotations per electron respectively.[21,66] We postulate that the greater electron-rotation coupling measured for dibutyl sulfide is related to that fact that the alkyl tails are more weakly coupled to the surface (as compared to the aforementioned smaller molecules), which leads to longer excited vibrational state lifetimes.[21,65-67] Importantly, during rotational excitation of the molecules which involved monitoring ~1,000 rotations at each voltage, translational events were not observed. This gives a rotational yield of >99.9%, making this a very selective process.

3.4 Conclusions

This study shows that the rotation of individual molecular rotors can be driven electrically using electrons from a scanning tunneling microscope tip. Above the threshold energy of the C-H stretch excitation, tunneling electrons are effective at selectively driving rotation but not translation of the thioether rotors.

The ability to rotate individual molecules on command will permit the interrogation of many important effects like rotational energy transfer along 1D molecular chains and rotational orientation switching in ordered arrays.

Chapter 4

Understanding the Mechanism of Rotation for a Single Molecule: STM and DFT Investigations of Dimethyl Sulfide Rotors on Au(111)

4.1 Introduction

Some theoretical studies[22,36,55,62,73] have helped to explain experimental observations of single-molecule rotation, but few are able to explain mechanisms of rotation for many of these complex rotor systems. This study examines a system similar to methane thiol on Au, using dimethyl sulfide on Au(111). Our previous thioether experiments showed that while symmetric dialkyl sulfides with chains of 2-6 carbons all had similar rotational barriers, dimethyl sulfide (with only 1 carbon in each of its chains) had a very low activation energy for its rotation. This study combines STM experiments and DFT calculations to investigate this low barrier for rotation and to reveal the mechanism of rotation for the simple thioether molecule, dimethyl sulfide (Me_2S).

4.2 Experimental Methods

Dimethyl Sulfide (≥ 99.0% purity) was obtained from Sigma Aldrich and was further purified by cycles of freeze/pump/thaw prior to introduction to the

STM chamber via a leak valve. Dimethyl sulfide was deposited onto the sample by a collimated molecular doser while the tip was scanning.

4.3 Theoretical Methods

A cutoff energy of 200 eV was used for the plane wave basis set. The Methfessel and Paxton method was used for smearing, with a width of 0.2 eV. The lattice constant for Au was calculated with these parameters and was found to be 4.182 Å, which is in good agreement with the experimental value of 4.078 Å. A 4 x 4 surface slab was used with 4 layers. The bottom two layers were fixed at bulk positions, but the top two layers were relaxed in order to simulate a surface. The Monkhorst-Pack scheme was used to sample the brouillon zone with a 2 x 2 x 1 kpoint mesh.

All of the geometry optimizations were performed with an energy based convergence criterion of 0.001 eV. All of the calculations were prepared with a spin-restricted method. Climbing image nudged elastic band (NEB) calculations were performed to calculate rotational barriers. NEB calculations calculated the barrier using a single image between neighboring equivalent sites within a rotational pathway. Further NEB calculations using additional images did not provide any extra insight into the barrier or the symmetry of the rotational potential.

4.4 Results and Discussion

Low temperature STM studies showed that Me_2S appeared hexagonal in shape on Au(111) (see Figure 4.1). This hexagon shape is due to a time-averaged superposition of multiple orientations with respect to the three-fold symmetry of the substrate. During the time-scale of one STM image (~2 mins), the rotor spent most of its time with its alkyl tails in six positions, corresponding to the six lobes seen in Figure 4.1a. In the instance of thioethers such as Me_2S, the alkyl tails rotate with the Au-S bond as their axle. Atomic resolution over a rotor showed not only the hexagonal rotor, but also resolved the Au lattice below the molecule. This high-resolution imaging allowed the adsorption site of the molecule to be estimated as roughly atop a Au atom (Figure 4.1b).

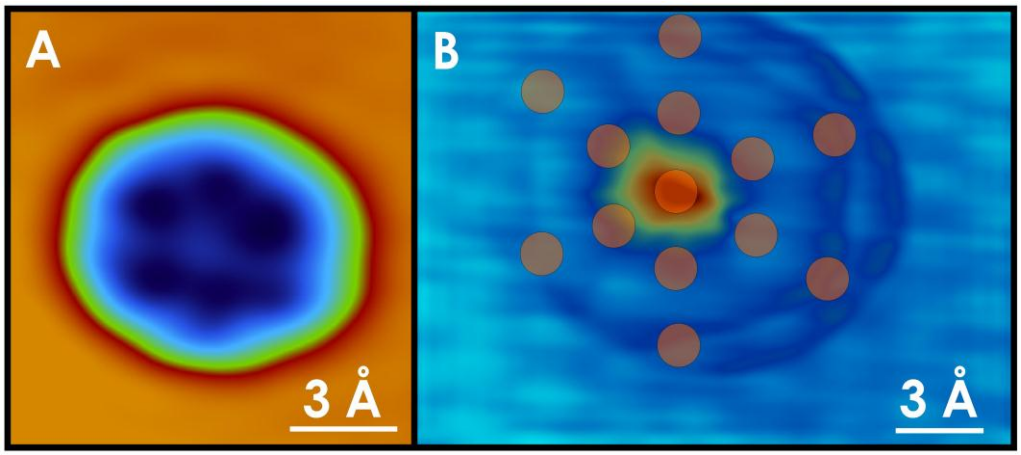

Figure 4.1: STM images of dimethyl sulfide. A) Dimethyl sulfide appears as a hexagon on a Au(111) surface due to a time-average of six equivalent orientations on the hexagonal surface (I= 1 nA, V_{tip}= 5 mV, Temp= 5 K). B) Atomic resolution over a dimethyl sulfide rotor shows that the center of the hexagon (which appears as a depression) appears to sit roughly atop a Au atom. The orange circles represent the positions of the underlying Au atoms. (I= 0.8 nA, V_{tip}= -200 mV, T= 7 K).

Even at very low temperatures (5-7 K) dimethyl sulfide appeared hexagonal, as it still rotated. As the molecule never stopped moving even at the lower limit of the instrumental temperature capabilities, it was not possible to calculate a torsional barrier experimentally. In order to elucidate this barrier to rotation, theoretical calculations were needed. Dimethyl sulfide was allowed to geometrically relax on a 4 x 4 Au slab with the S atom directly above each of the traditional adsorption sites (atop, bridge, hcp three-fold hollow and fcc three-fold hollow). In this way the minimum energy adsorption site was found from the atop site relaxation (see Figure 4.2). Energies normalized to the relaxed atop structure were found to be 280, 280 and 310 meV higher for the hcp hollow, fcc hollow and bridge structures, respectively.

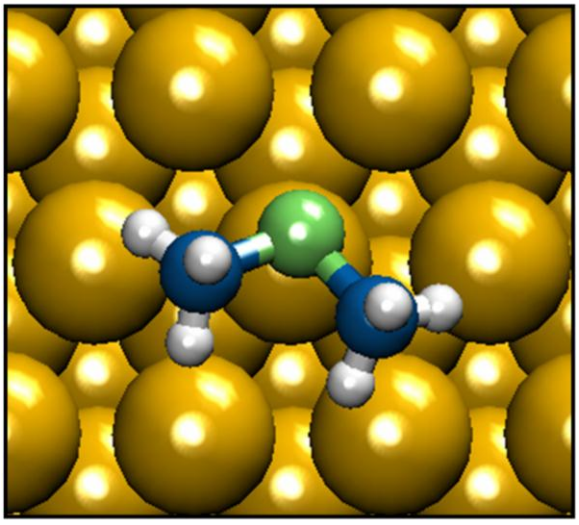

Figure 4.2: DFT adsorption site prediction. After relaxing the dimethyl sulfide molecule on atop, bridge, hcc and fcc three-fold hollows it was found that the minimum energy adsorption site is near atop. This adsorption site (shown above) is not directly above any one traditional adsorption site, but is closest to atop a Au atom.

While examining the calculated adsorption site (Figure 4.2) it became apparent that while Me_2S is close to atop a Au atom, it is not directly on any of the traditional adsorption sites. If the molecule were to rotate about a stationary Au-S bond at this adsorption site, its rotation would not reproduce the hexagonal shape seen in STM imaging (see Figure 4.1). In order to replicate the symmetry seen experimentally, the S atom must also change position in some manner. In order to understand the mechanism of rotation, three possible pathways were examined; to create the three-fold symmetry observed with STM, the S atom could sample three equivalent orientations as it rotated around: a) a hcp three-fold hollow, b) a fcc three-fold hollow or c) atop the same Au atom (see Figure 4.3). In each of the panels of Figure 4.3 the S atom positions have been shown for 0°, 120° and 240° rotations along each pathway. In each case the alkyl tails would rotate around the center of the pathway as the S atom precessed.

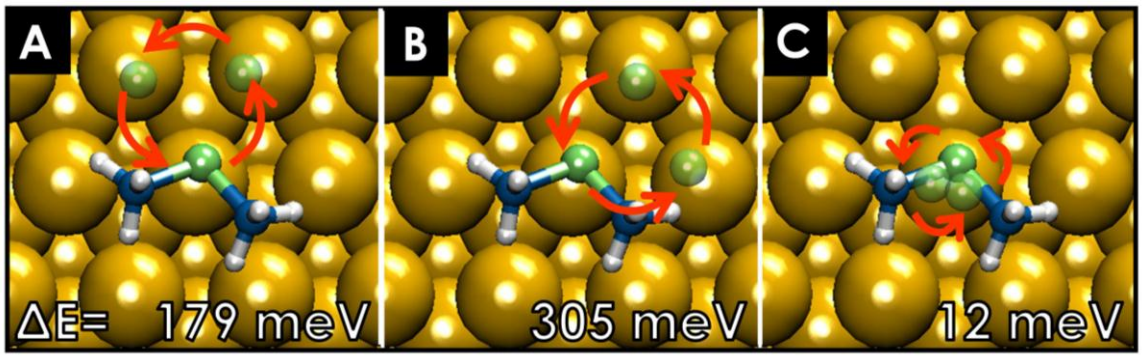

Figure 4.3: DFT rotation of dimethyl sulfide. Nudged elastic band calculations were performed to calculate barriers for the three possible pathways which were considered; Rotational barriers around A) a hcp 3-fold hollow, B) a fcc 3-fold hollow and C) a Au atom were calculated to be 179 meV, 305 meV and 12 meV, respectively. Opaque green atoms represent the positions of the S atom at rotation positions of 0°, 120° and 240° as it would precess around the different paths. The alkyl tails would rotate as the S precessed.

Climbing image nudged elastic band (NEB) calculations were used to calculate the torsional barriers for each of the three pathways. Torsional barriers for rotation around a hcp three-fold hollow, a fcc three-fold hollow, and atop a Au atom were calculated to be 179 meV, 305 meV and 12 meV, respectively. These calculations showed that, while barriers to rotate around either of the three-fold hollow sites were too high to make those pathways reasonable, the barrier for rotating around a Au atom was extremely small. NEB calculations with more images revealed that the barrier was indeed very small, and was very much at the limits of DFT capability. This extremely small theoretical barrier is consistent with the experimental observations that even at 5 K the molecules still rotated. Furthermore, the precession of the S atom around the top of a Au atom is further evidenced in STM imaging (Figure 4.1b). Images showing the time-averaged superposition of the Me_2S rotor showed the molecule to be roughly

atop a Au atom. If the positions of a Me_2S molecule precessing around the top of a Au atom were superimposed on one another, the resulting time-averaged hexagon would appear to be atop as the center of this pathway is directly atop a Au atom.

4.5 Conclusions

STM imaging showed that a small, thioether rotor (dimethyl sulfide) had a very small barrier to rotation and rotated even at low temperatures (5-7 K). DFT calculations revealed that the minimum energy adsorption site for this molecule on Au was actually not directly above any of the traditional adsorption sites, but was closest to being atop. Using nudged elastic band calculations to calculate the torsional barriers for three possible rotational pathways, it was found that the most likely pathway for Me_2S rotation was for the S atom to precess atop a Au atom while the alkyl tails rotated. This mechanism for rotation supported the experimental results that the barrier to rotate was extremely small, and the center of the rotational path was atop a Au atom. Understanding the pathway to rotation in such a system will allow crucial insight when trying to develop systems in which to study controlled, directional motion of a rotor or rotational coupling between adjacent molecules.

Chapter 5

Chirality and Rotation of Asymmetric Surface-Bound Thioethers

5.1 Introduction

Recently, thioether linkers have proven effective in promoting enantioselectivity in heterogeneous catalysis by anchoring chiral modifiers to nanoparticles,[74] and asymmetric thioether intermediates have shown high enantioselectivity.[75] Little is known, however, about how the thioether functionality binds to surfaces.[76] Controversies over alkane thiol-metal interface structures[77-79] exemplify the value of a detailed atomic-level understanding of all similar molecule-surface interactions. Asymmetric dialkyl sulfides have two prochiral lone pairs on the central sulfur atom and therefore, may be expected to exhibit surface-bound chirality.[80-85] The earliest picture of a dialkyl sulfide-surface interaction predicted an upright geometry.[42] Despite the fact that the arrangement of the two alkyl groups and lone pairs around the central S atom on dialkyl sulfides is tetrahedral, it appears that the chirality of surface-bound asymmetric alkyl sulfides has not previously been discussed. This work uses a combination of density functional theory (DFT) and scanning tunneling microscopy (STM) to investigate the adsorption of an asymmetric dialkyl sulfide, butyl methyl sulfide, on a Au(111) surface.

5.2 Methods

5.2.1 Experimental Methods

Butyl methyl sulfide was obtained from the rare chemical library of Sigma Aldrich and was further purified by cycles of freeze/pump/thaw prior to introduction to the STM chamber via a leak valve. Purity was verified with mass spectra and STM imaging. After depositing butyl methyl sulfide at 5 K the sample was heated to ≥30 K to ensure that all molecules had sufficient energy to reach their equilibrium adsorption sites. Alternatively a given area could be "locally electrically annealed" by scanning over the molecules at 500 pA and 400 mV, which also equilibrated molecules to their preferred adsorption sites.

5.2.2 Theoretical Methods

The geometries of the structures in these calculations were relaxed using a conjugate gradient algorithm until the forces on all the unconstrained atoms were less than 0.03 eV/Å. All surface calculations used supercells defined using the DFT-optimized Au lattice constant, 4.182 Å. Au(111) was represented as a slab four layers thick with the bottom two layers constrained in its bulk positions. A vacuum spacing of 14 Å was used in the direction of the surface normal for all calculations. In order to avoid the interactions between adsorbates, all calculations were performed for a coverage corresponding to one molecule per supercell, that is, with an area of 121 $Å^2$/molecule using a (4×4) surface unit

cell. All calculations used a 3×3×1 Monkhorst-Pack *k*-point mesh which was sufficient to give well-converged results. The fcc termination is dominant in terms of area exposed in the 22 x √3 Au(111) reconstruction, hence, a fcc slab was used in all DFT calculations. When examining adsorption, molecules were placed on only one side of the slab. Dipole corrections were therefore applied in computing all of the energies reported below.[86,87] The nudged elastic band (NEB) method[88,89] was employed to investigate the energy barriers for both rotation and inversion of butyl methyl sulfide adsorbed on Au(111). The total number of intermediate images for each NEB calculation was 5.

5.3 Results and Discussion

5.3.1 Asymmetric Dialkyl Sulfide Attachment: Chirality of the Adsorbed Species

When adsorbed on Au(111) at low coverages and annealed to ensure equilibration, the chirality of butyl methyl sulfide molecules can be inferred by their appearance in STM imaging. Figure 5.1a shows two mirror image pinwheels, which are the two surface-bound enantiomers of the otherwise achiral butyl methyl sulfide molecule. The pinwheel shape of these molecules is due to their rotation about the central Au-S bond[37,62,90,91] and their preferred orientation in one of the six near-equivalent directions on the Au(111) surface (the rotational properties of these molecules are discussed in section 7.3.2). The asymmetric sulfide molecules attach to the Au surface through one of the two

lone pairs on the sulfur and, depending on which of these lone pairs binds, determines the surface-bound chirality of the molecule (Figure 5.1b).

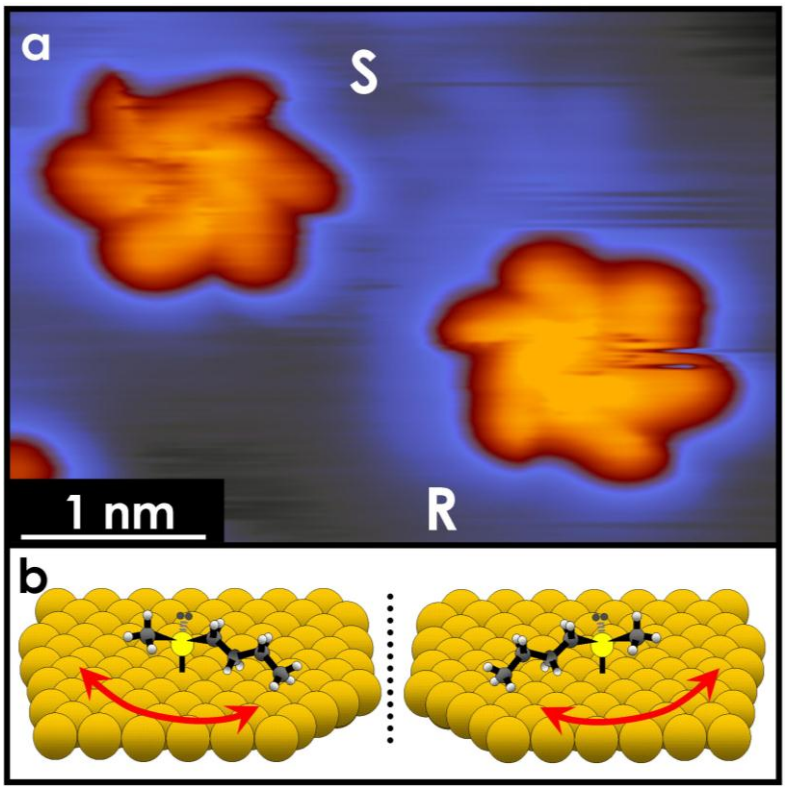

Figure 5.1: Two butyl methyl sulfide molecular rotors of opposite chirality. a) The surface-induced chirality is apparent, as they are imaged as mirror- image pinwheels as they rotate about the central Au-S bond. Even though the temperature is low (5 K), the molecules rotate under perturbative tunneling conditions. (I = 400 pA, V = 300 mV, 5 K). b) Schematic representation of the adsorption of the two enantiomers and their rotation about their central Au-S bond.

DFT reveals that, consistent with STM images, adsorption on the Au surface gives the possibility for mirror symmetry of the adsorbed species. Figure 5.2a shows the calculated minimum energy adsorption site. Identification of this configuration was approached in a systemic way; the calculations were first performed with 11 initial configurations that varied tilt angle of the molecule by

increments of 5° in the direction of the surface normal. Using the most stable configuration obtained from these calculations, a new set of initial configurations were then generated by rotating the molecule in the surface plane by increments of 10°. In total, therefore, 22 initial configurations were considered for the butyl methyl sulfide around the atop site of Au atom. Since previous calculations for the dimethyl sulfide adsorption on Au(111) demonstrated that the atop site is ~0.3 eV more favorable than the fcc, hollow, hcp hollow, and bridge site[91], these kinds of intensive calculations for the butyl methyl sulfide molecule were focused only on adsorption near the atop site of Au atom. Charge calculations by Bader analysis[92-94] shows that upon this adsorption, a charge of -0.11e is transferred to the surface from the butyl methyl sulfide, indicating that in simple terms, adsorption to the surface occurs via binding of one of the lone pairs on the S atom. A charge density plot (Figure 5.2b) shows the non-bonding lone pair of the sulfur pointing off to the side of the molecule, which confirms that the molecule maintains its tetrahedral shape. With this geometry essentially unperturbed, attachment to the surface breaks the symmetry plane found in gas-phase molecule and yields the chirality of the surface-bound molecules.

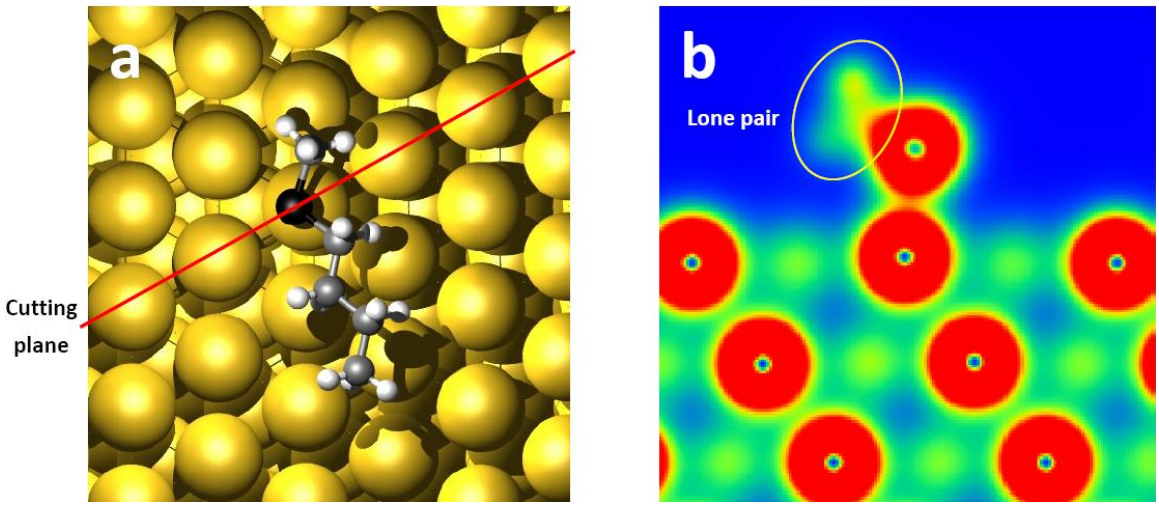

Figure 5.2: a) The most stable DFT-optimized geometry of adsorbed butyl methyl sulfide on Au(111) and b) its charge density contour map. The cutting plane for creating this map is also shown in a).The position of the non-bonding lone pair is circled. The uppermost atom in red is the S atom, not to be confused with the other Au atoms (red) in the Au lattice.

Using further DFT calculations, it was found that the barrier to inversion between the energetically equivalent enantiomers was 0.24 eV (Figure 5.3). This relatively high barrier is not surprising, as the molecule must switch which lone pair binds to the surface in order to invert its chirality. This high barrier is also evidenced with STM experiments, as the rotors were not observed to switch chirality under normal scanning conditions at either 5 or 78 K. Only with high energy electrons (>0.4 eV) supplied by the STM tip was it possible to overcome the high barrier to inversion and invert the chirality of the adsorbed molecules.[67,68]

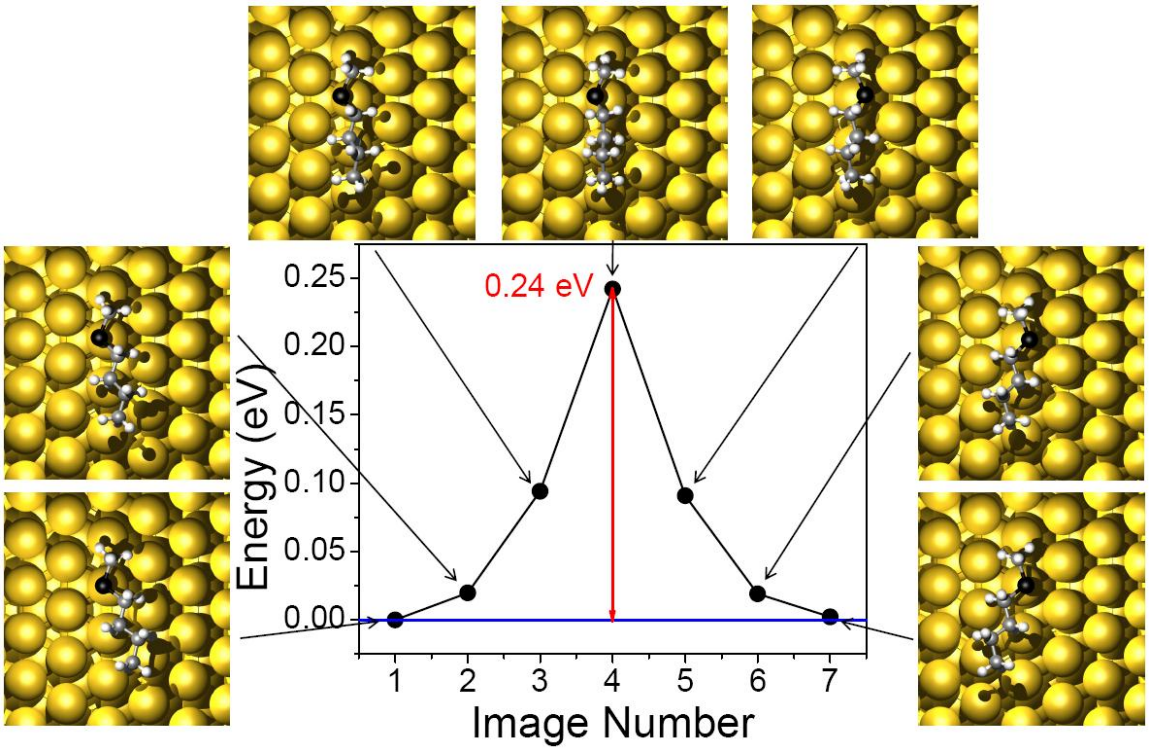

Figure 5.3: Nudged elastic band results for the inversion barrier between the energetically equivalent enantiomers. The inversion pathway for the adsorbed butyl methyl sulfide on Au(111) is exhibited along with each corresponding energy state. The barrier to this inversion is 0.24 eV.

5.3.2 Observed Rotational Properties of the Adsorbed Molecules

Both R and S enantiomers of butyl methyl sulfide rotate around their central Au-S bond axis. The six lobes of the chiral pinwheels shown in Figure 5.1 are due to the time-averaged superposition of six equivalent orientations of the molecule with respect to the underlying hexagonally-packed surface. As shown in the DFT minimized structure in Figure 5.2a, the butyl methyl sulfide molecules adsorb slightly off center of the traditional atop Au site. This off center adsorption requires the S atom to precess as the molecule rotates in order to reproduce the six-fold symmetry seen in the STM images. The calculated

maximum radius for the rotation of the S atom in the surface plane with respect to a center of a Au atom was 0.47 Å. This off-axis rotation has been characterized before[91], and explains the pinwheel appearance as opposed to a simpler hexagonal shape for the asymmetric sulfide molecule. The minimized structure calculated by DFT also allows for absolute chirality assignment of the surface-bound molecules based on the priorities around the central S atom of 1) the Au surface, 2) the butyl tail, 3) the methyl tail and 4) the unbonded lone pair. This approach was used to assign the absolute chirality of each molecule in the STM image in Figure 5.1.

It is possible to induce the rotation of these molecules either by adjusting the tunneling conditions or by heating the surface. As the 22 x √3 reconstruction of Au(111) leads to alternating regions of hcp and fcc atoms which can affect the preferential binding of adsorbates, molecules in both areas were studied independently. Figure 5.4 shows R and S molecules in both the hcp and fcc regions of the Au(111) surface. Molecular rotation can be induced even at 5 K by using perturbative imaging conditions (higher currents and voltages - top row of Figure 5.4), whereas lower currents and voltages allow for the molecules to be imaged as static, crescent-shaped molecules while they are not spinning (middle row of Figure 5.4). The crescent shape of the molecule is supported by the DFT calculations (see Figure 5.2a), where the tails are calculated the tilt toward the surface rather than perpendicular to the Au substrate. At even slightly elevated

temperatures the molecules have enough energy supplied by the temperature of the surface to rotate (bottom row of Figure 5.4). No noticeable differences were found between the rotational properties of rotors adsorbed in the fcc and hcp regions of the Au surface.

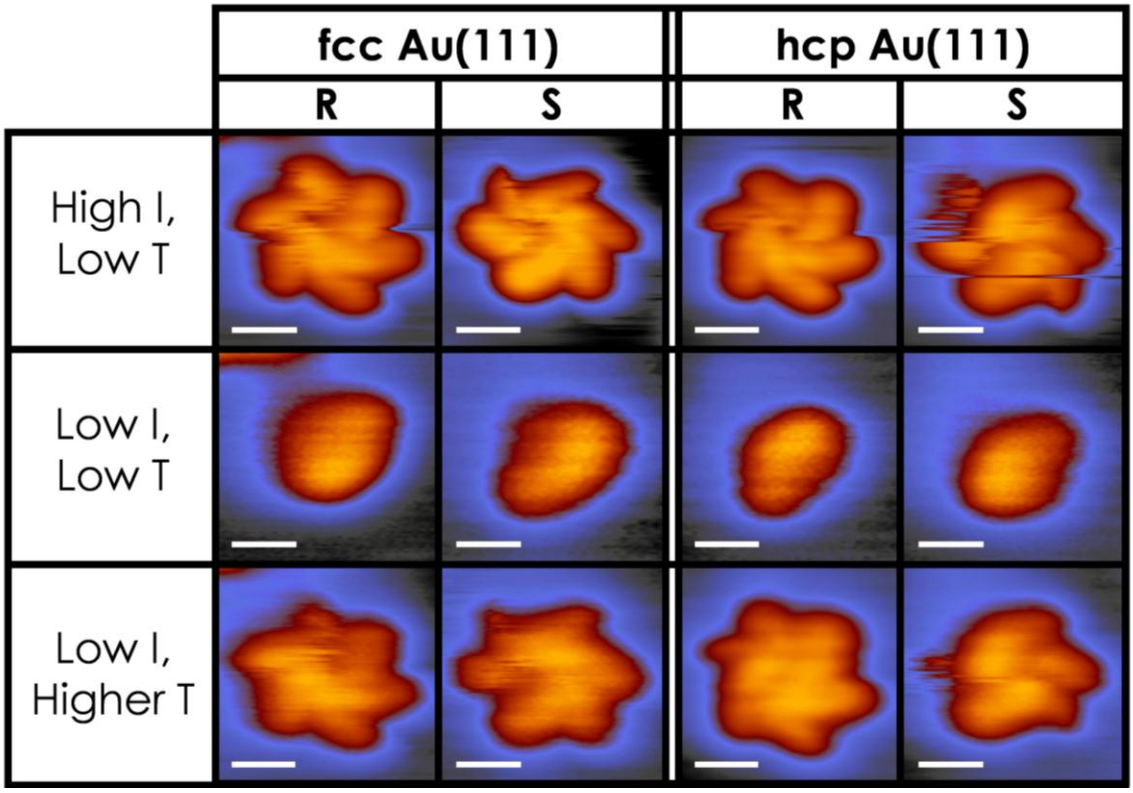

Figure 5.4: STM images of rotating and static R and S butyl methyl sulfide molecules in the fcc and hcp regions of the Au(111) surface. Top row: rotation caused by perturbative imaging conditions (higher tunneling currents and voltages). Middle row: static molecules under non-perturbative imaging conditions (low current and voltage). Bottom row: molecules rotating at non-perturbative imaging conditions due to a sample temperature increase from 5 to 10 K. (Tunneling conditions – top row: 300 pA, 300 mV, 5 K; middle row: 2 pA, 50 mV, 5 K; bottom row: 5 pA, 50 mV, 10 K.) Scale bars = 0.5 nm.

STM also affords the option to measure the rotational rates of these molecules. If the STM tip is placed to the side of one of the molecule's lobes, all

six positions of the butyl tail with respect to the underlying surface can be distinguished. In this measurement the feedback loop (which is normally used to modulate the STM tip height in order to maintain a constant tunneling current) is turned off and the tunneling current in monitored with respect to time (*I* vs. *t*). Six current states can be measured, for the six positions of the molecule with respect to the hexagonal Au surface (Figure 5.5). These states are a reflection of the proximity of an alkyl tail of the rotor molecule to the STM tip (the closer the tail, the higher the tunneling current).

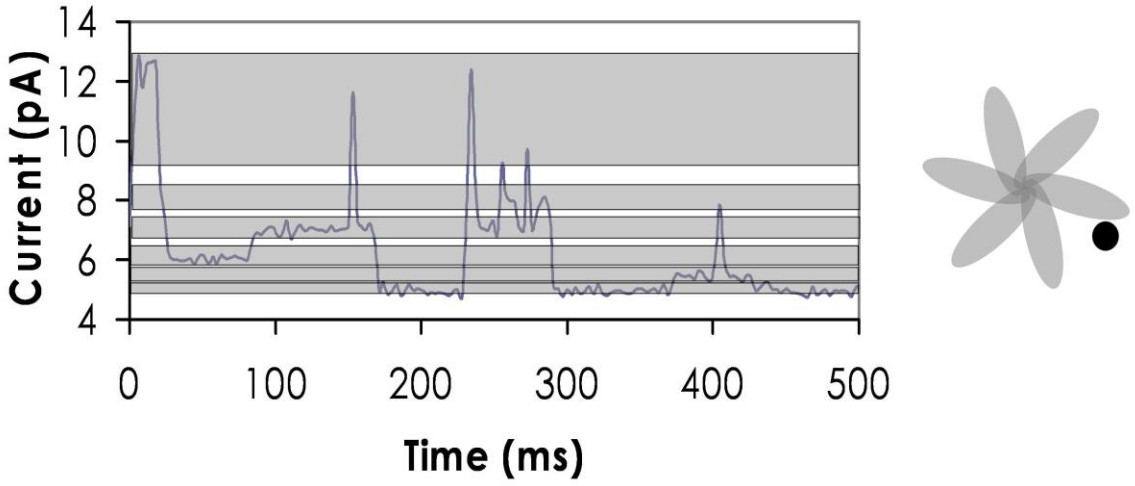

Figure 5.5: Current vs. time (I vs. t) curve shows rotational events as switches between six discrete current states. These states are due to six possible orientations of the molecule with respect to the STM tip. (Tunneling Conditions: I = 5 pA, V = 380 mV, 5 K).

By measuring how fast the alkyl tail changes position (and hence the rotational rate) as the temperature is increased, it is possible to further understand the rotational energetics (Figure 5.6). Arrhenius data is shown for a

single butyl methyl sulfide molecule in the fcc region of the Au(111) surface. (The fcc and hcp regions show similar rotational energetics within experimental uncertainties). The activation energy (E_a) and the attempt frequency (A) calculated from these results are also displayed in Figure 5.6. All rates are calculated by measuring the number of switching events during the course of *I* vs. *t* curves. The attempt frequency is noticeably low compared to expected molecular event frequencies, however, this low attempt frequency has been observed previously for single molecule rotors. It has been postulated that the low A values arise due to multiple configurations of the alkyl tails in the ground state that lead to entropic effects in the transition state.[95-97]

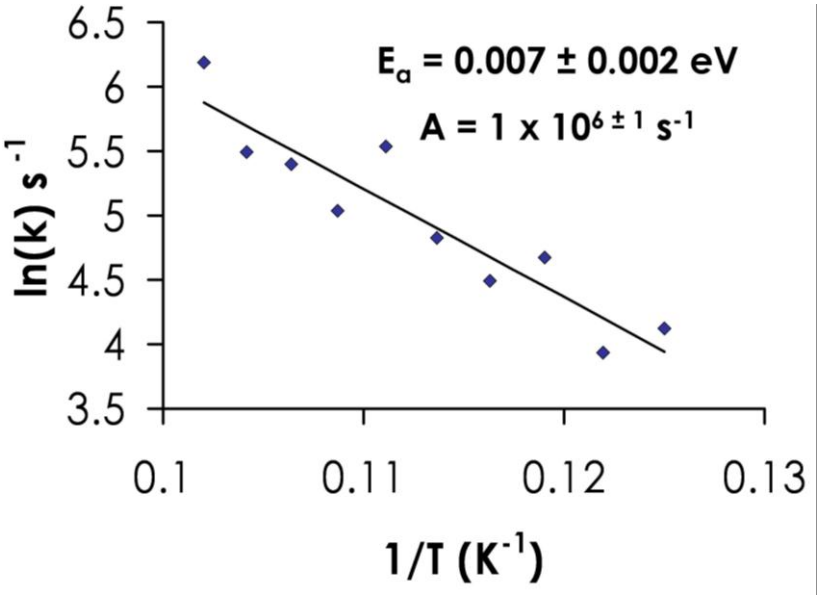

Figure 5.6: Arrhenius plot for a butyl methyl sulfide rotor. (Tunneling conditions: I = 5 pA, V = 100 mV).

To model the rotational barrier and further understand the shape of the rotating molecule, additional DFT calculations were performed. NEB calculations yielded a rotational energy barrier of 0.03 eV for a pathway involving precession of the S atom around the top of an Au atom (see Figure 5.7). Other possible pathways were ruled out because they gave much higher rotational barriers.

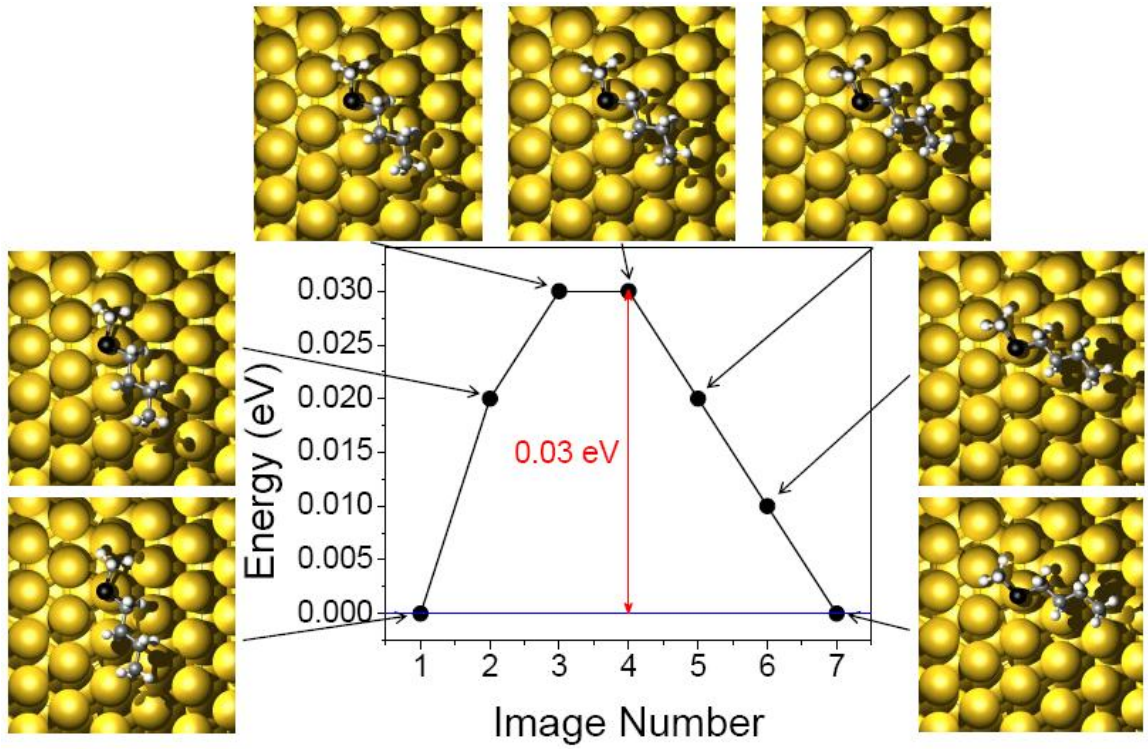

Figure 5.7: Nudged elastic band results for the rotational barrier of the S atom around the top of a Au atom. The rotation of this molecule by 60° was enough to cover the whole rotational path. The final state is equivalent to the initial state rotated by 60°. The rotational pathway for the adsorbed butyl methyl sulfide on Au(111) is exhibited along with each corresponding energy state. The barrier to this rotation is 0.03 eV.

The rotational energy barrier predicted by the DFT calculations is similar in magnitude to experimental observations, but the DFT barrier is ~4 times

larger. Two caveats must be applied when quantitatively comparing these barriers. First, accurately resolving energy differences at the level of 0.01 eV is a challenging standard for any kind of quantum chemistry calculation, so it is perhaps unreasonable to expect that these calculations can make any statement more precise than confirming that the rotational energy barrier is small. Second, DFT calculations of the kind do not accurately account for dispersive interactions. For the dialkyl sulfide considered here, dispersive interactions between the molecule and the surface could vary slightly between the minimum energy state and the transition state for rotation, contributing to the net barrier for rotation. DFT calculations including semi-empirical corrections for dispersion are now available[98], but these methods are still subject to the challenge of precisely evaluating small energy differences discussed above.

5.4 Conclusions

Surface-bound butyl methyl sulfide molecules were studied using STM and DFT. This combination of experiment and theory allowed the equilibrium structure, rotational properties, and the barrier to rotation to be determined. Furthermore, high-resolution imaging revealed that the symmetry of the achiral molecule is broken upon adsorption to a surface. As the molecules bind to the surface primarily through just one of the lone pairs on the S, their tetrahedral geometry is preserved and this leads to the appearance of two surface-bound

enantiomers. DFT reveals that the barriers to inversion between the enantiomers are fairly high. This study indicates that the Au-sulfide bonds commonly used in organic, inorganic and materials chemistry can in fact have a chiral nature. Understanding the atomic-scale geometry and associated chirality of the Au-sulfide bond will make it easier to predict the surface properties of thioether linkers and will highlight the possibility for diastereomeric effects when chiral sulfides are used.

Chapter 6

Dynamics of Molecular Adsorption and Rotation on Non-Equilibrium Sites

6.1 Introduction

While it is known that reactions can be adsorption site dependent[99,100], it is most often assumed that molecules occupy equilibrium sites when adsorbed on surfaces. This is not always the case, for example, on crowded surfaces molecules can be forced to adopt less energetically favorable sites.[101] A few careful studies have shown reaction dependence on adsorption site[99,100], as well as site-dependent diffusion[100,102], adsorption[103-107] and lateral forces[108-110]; however in most cases very little is known about mechanisms for diffusion between adsorption sites. It has also been demonstrated that molecules with multiple attachment sites to a surface can exhibit a mismatch with the surface lattice. This forced binding to non-equilibrium adsorption sites can lead to highly directional diffusion properties.[111]

Since intermediate or precursor states often only exist on the surface in small quantities or for short periods of times, it is very difficult to study their physical properties.[112,113] Using STM it is possible to monitor the properties of these non-equilibrium or precursor species on a molecule-by-molecule basis[114], and if imaging conditions are chosen carefully, metastable species can be imaged

without being perturbed.[115,116] Previous studies have used step edges and defects to trap molecules[117,118]; however we have chosen a molecule which is trapped in multiple metastable adsorption sites on terraces when deposited at low surface temperatures. The molecule under consideration in this paper is butyl methyl sulfide, which is a simple asymmetric thioether (RSR') molecule. This molecule and others like it have been studied as molecular rotors; however only equilibrated molecules have been considered in previous studies.[37,62,90,91,97,119] As precursor-adsorbed molecules do not have enough energy to make it to their preferred sites (which are most likely <1 Å away), we are able study the rotational and equilibration behavior of these metastable molecules and relate these properties to each molecule's adsorption site. Herein we report data for the same chemical species in three metastable adsorption sites and their subsequent equilibration to a single site as a function of either applied bias voltage or temperature. Using STM, it is also possible to show the differences in physical properties of this molecule at all four adsorption sites, including rotational rates and appearance in STM images. From these measurements a relative energy landscape is proposed for each adsorption site, and a correlation is drawn between rotational barrier and adsorption energy.

6.2 Experimental Methods

Butyl methyl sulfide was obtained from the rare chemical library of Sigma Aldrich and was further purified by cycles of freeze/pump/thaw prior to introduction to the STM chamber via a leak valve. Purity was verified with mass spectra and STM imaging. Butyl methyl sulfide was deposited onto the cold sample by a collimated molecular doser while the tip was scanning.

6.3 Results and Discussion

When dosed at low coverage (<0.3 ML) and at 5 K on Au(111), thioether molecules (including butyl methyl sulfide) do not preferentially adsorb in any region of the Au herringbone reconstruction, or even on any preferred adsorption site. Figure 6.1 shows a large-scale STM image of an initial dose of butyl methyl sulfide (left) as well as the same area of the surface after all of the molecules have been equilibrated (right). While initially there appear to be four types of species on the surface, after supplying electrical energy to the molecules from the STM tip it is clear that they are all of the same molecular identity. The insets in Figure 6.1 show zoomed-in images of the four as-dosed adsorbed species, which are assumed to image differently due to their different adsorption site on the underlying Au surface. These four sites are labeled as α, β, γ and δ, and butyl methyl sulfide molecules are seen to rotate about their central S-Au bond at perturbative tunneling conditions when adsorbed on any of these four

sites. At elevated tunneling currents and low bias voltages the STM tip is brought extremely close to the sample, and will interact very strongly with the adsorbed species. In this case, the STM tip perturbs the molecules on the surface which causes molecular rotation at lower than normal temperatures for these molecules.

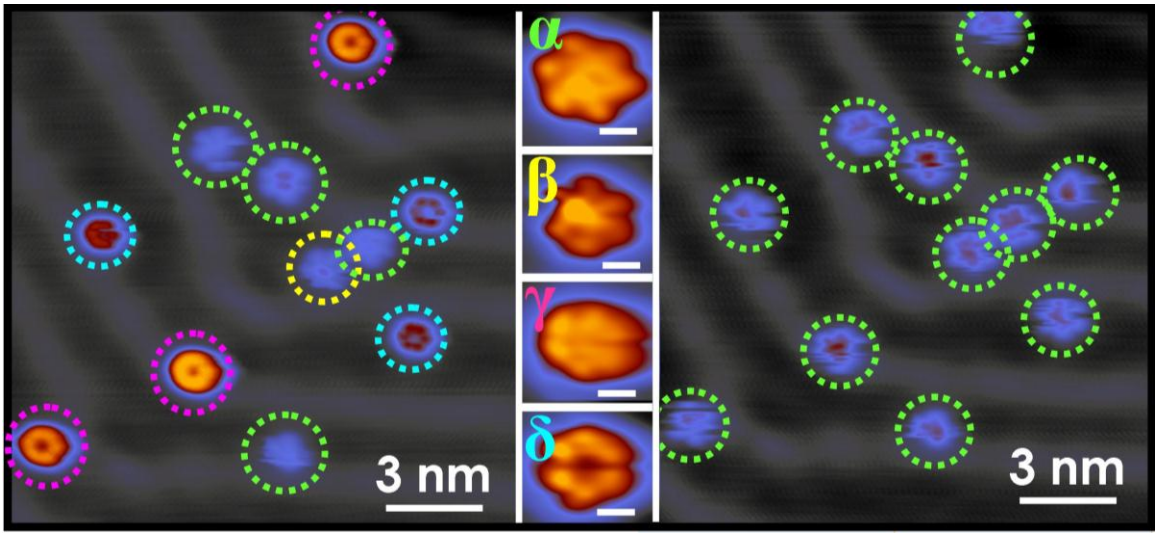

Figure 6.1: STM images of butyl methyl sulfide rotors on Au(111). The different adsorption site of each molecule leads to different rotational properties and different appearance in STM imaging. Left: as-dosed collection of molecules on Au(111) appear as if there are four types of molecule present. Insets in the middle show high-resolution images of each type of species. After supplying energy to the molecules via the tunneling current from the STM tip (right) it is seen that all molecules are indeed the same, and have all converted to their global minimum energy site, which is labeled here as α. The slight differences in contrast observed on the right are due to the natural 22 x √3 reconstruction of the surface. (Tunneling conditions: left and right: 300 pA, 100 mV, 7 K; Inset: α, β and δ: 700 pA, 50 mV, 5 K; γ: 5 pA, 50 mV, 5 K). Scale bars in insets = 0.5 nm.

Molecules in all of the adsorption sites can be distinguished based on their distinctive contrasts and shapes upon STM imaging. Measured diameters of 2.3, 2.3, 3.0, and 2.3 nm and apparent heights of 0.10, 0.10, 0.23, and 0.15 nm were

found for α, β, γ and δ species, respectively. While α and β species imaged with the same dimensions, close inspection of these species in Figure 6.1 shows that their hexagonal outlines are offset 30° from one another. It should be noted that these measured dimensions are partially STM tip dependent and do not represent the exact dimensions of the rotating molecules; however, comparisons of species for many hundreds of molecules imaged with many tip states support these general, relative characteristics.

We have observed no accumulation at more favorable sites such as step edges, which supports our hypothesis that when deposited on the surface at 5 K these molecules cannot equilibrate to their preferred adsorption sites. Figure 6.2 shows a step edge after dosing butyl methyl sulfide at 5 K. While there are a couple of molecules that have adsorbed directly at the step, there are also molecules very close to the step that have not diffused to it. Step edges are very attractive sites for adsorption due to the under-coordination of the metal atoms and it has previously been postulated that an accumulation of molecules at a step edge should occur if adsorbed species have low barriers to diffusion.[120] We have previously shown that similar thioether molecules aggregate at step edges at temperatures as low as 80 K.[39,40]

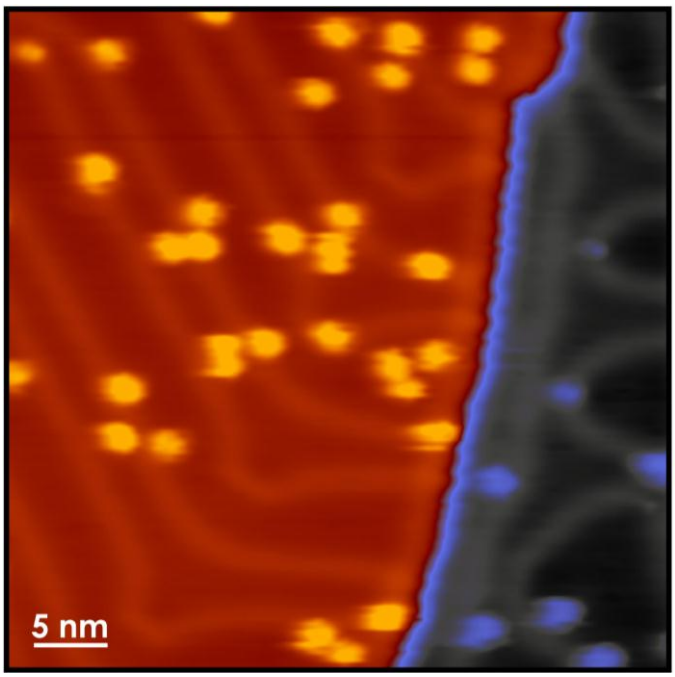

Figure 6.2: Butyl methyl sulfide molecule distribution in proximity to a step edge. Molecules appear randomly distributed across the surface above and below the step edge. Two molecules sit close to the step edge (which offers under-coordinated Au atoms and therefore favorable sites for adsorption), however other molecules adsorb very close to the step without moving onto it, which supports the conclusion that these molecules do not have enough energy to diffuse along the surface and essentially adsorb very close to where they land. (Tunneling Conditions: I= 250 pA, V= -300 mV, T = 7 K)

Interconversion between adsorbed species was studied as a function of temperature and bias voltage. These conversions, which are the equilibration of a given molecule to its preferred adsorption site, are represented in Figure 6.3. As can be seen in Figure 6.1, these molecules only need to move a very small distance to equilibrate (<1 surface lattice spacing), and this lateral displacement is almost indistinguishable in the before and after images such as those in Figure 6.1. It can be seen from Figure 6.3 that the α species were at the lowest energy sites, which is consistent with previous studies of the equilibrium adsorption site

of this rotor molecule.[119] β rotors were also very stable and exhibited high electrical and thermal barriers for equilibration to α rotors, while γ and δ rotors were less stable and could be equilibrated at lower temperatures and voltages. By increasing the voltage while keeping the tunneling current constant, progressively higher energy electrons were supplied to the molecules under investigation. Molecules were imaged in this incremental manner until a change in adsorption site occurred. This type of scan "locally annealed" the surface by supplying energy only to the molecules within the area of the image. The same process was performed as a function of temperature, wherein the entire surface was annealed to investigate the thermal equilibration of the metastable species. Using the combination of these thermal and electrical treatments, it was possible to deduce both the true equilibrium site (α) and the relative stability of the metastable adsorption sites ($\gamma < \delta < \beta$).

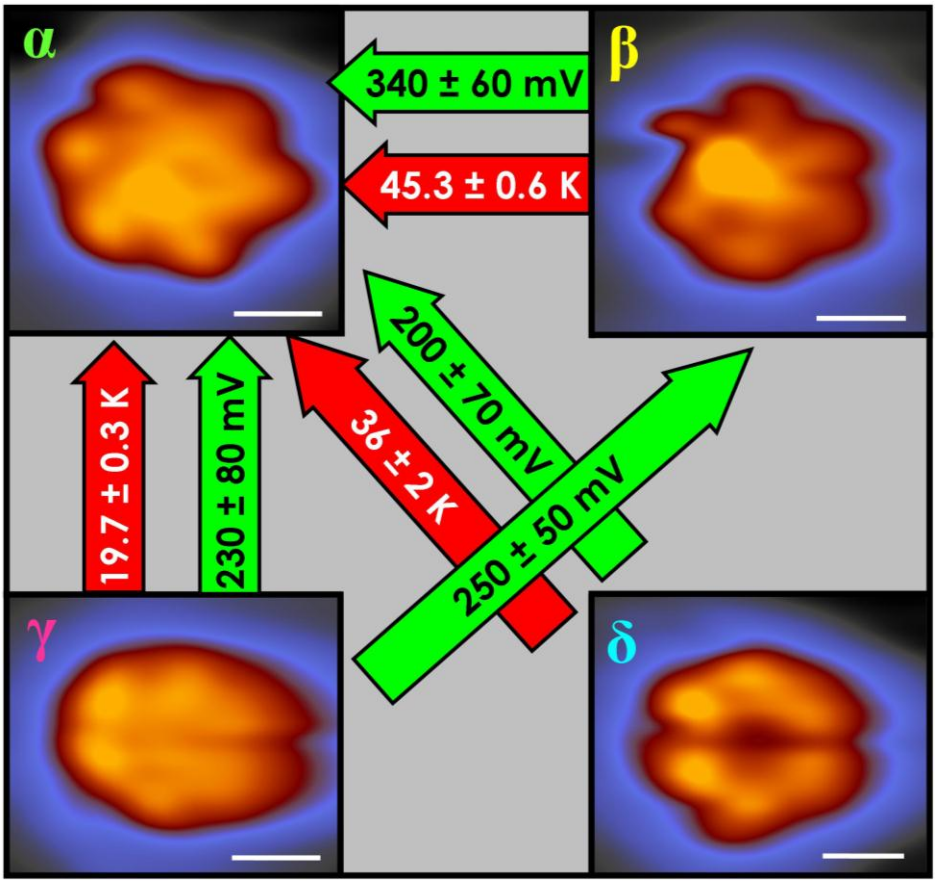

Figure 6.3: Interconversion between adsorption sites as a function of temperature (red arrows), and voltage (green arrows). Scale bars = 0.5 nm. Tunneling currents were kept at 100 pA for electrical measurements, and 5 pA and 50 mV were used for thermal measurements.

To further understand the properties of butyl methyl sulfide in its unequilibrated states, the rotational properties of all the adsorbed species were studied. At non-perturbative tunneling conditions most of the rotors did not spin at 5 K; only the γ rotors continued to spin at such a low temperature (see lower images in Figure 6.4 for static α, β and δ rotors). The temperature was then increased at non-perturbative imaging conditions until the rotors appeared to be spinning on the timescale of STM imaging (~1-10 s to image a molecule). Figure

6.4 shows the temperatures at which rotation began for all the adsorbed species. Within error all but the γ-adsorbed rotors began to spin at the same temperature of ~8.5 K. This rotational onset temperature is a crude way to measure the thermal barrier to rotation,[37] however a more accurate measurement of this barrier utilizes Arrhenius plots, which are described in the following paragraphs.

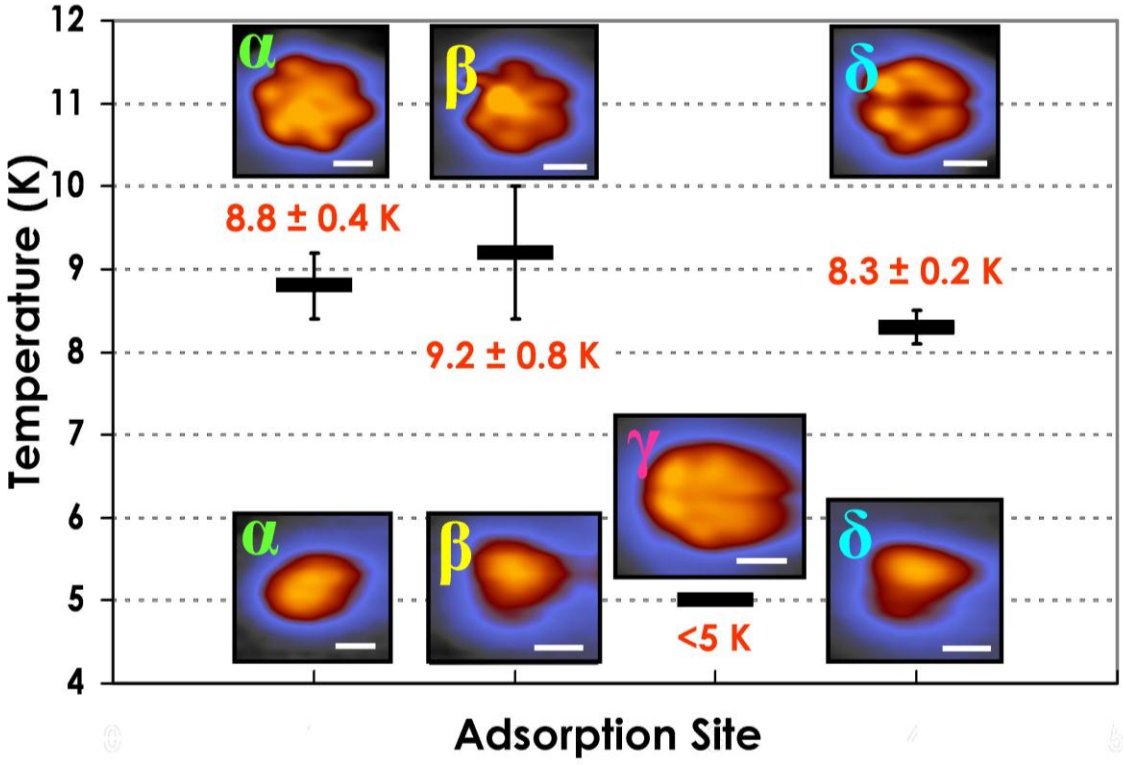

Figure 6.4: Onset of rotation for the four adsorption sites. Top images: rotating molecules, bottom images: static molecules (except γ) at low temperatures recorded at non-perturbative tunneling conditions. It was not possible to observe static γ-adsorbed molecules, even at 5 K, so their rotational onset temperature is listed as < 5 K. (Tunneling Conditions: Top images: 700 pA, 50 mV, 5 K; bottom images (including γ): 5 pA, 50 mV, 5 K. Scale bars = 0.5 nm.)

By measuring the rotational rate in *I* vs. *t* curves as the temperature is increased, it is possible to generate Arrhenius plots to further understand the

rotational energetics and specifically the torsional barriers of the butyl methyl sulfide molecules at different adsorption sites (Figure 6.5). It is also important to note that these molecules are assumed to have rotational properties which are independent from the reconstruction of the Au(111) surface. Our previous molecular rotor studies have shown that thioethers such as butyl methyl sulfide have very similar rotational energetics on hcp and fcc regions of the surface[119], so the hcp and fcc regions can be considered nearly identical and precautions were taken to ensure that molecules were not directly on top of the soliton walls that separate hcp and fcc regions.

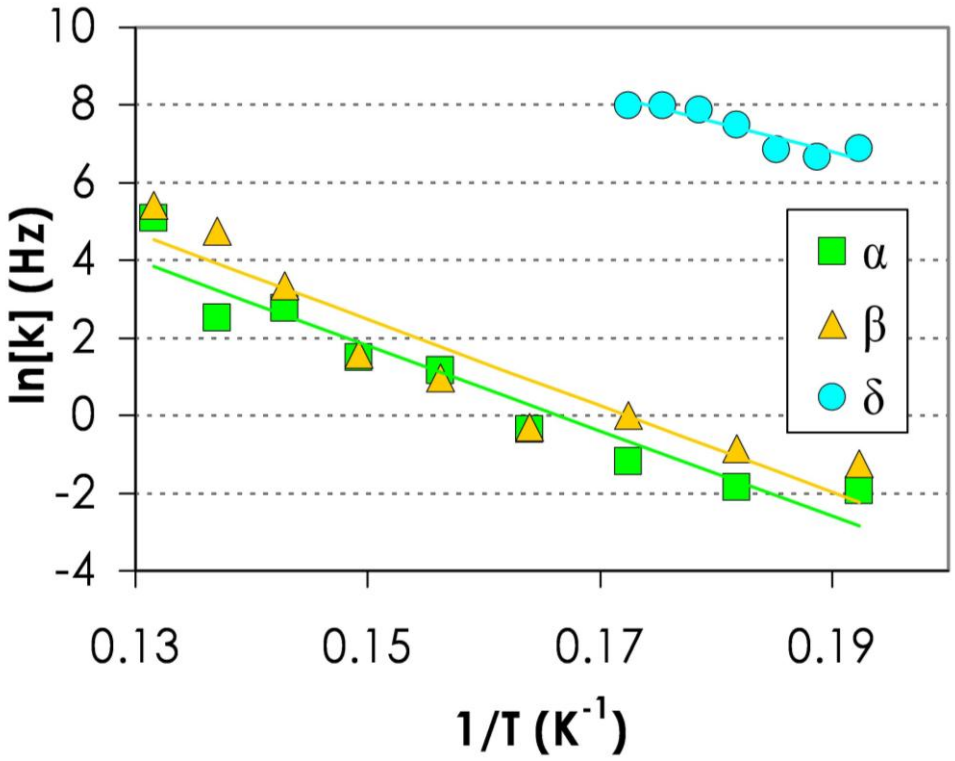

Figure 6.5: Arrhenius plots for adsorbed rotors in α, β and δ adsorption sites. γ-adsorbed molecules rotated too quickly to measure even at 5 K, therefore no points are shown for molecules at this adsorption site. All *I* vs. *t* measurements were recorded at 5 pA, 100 mV.

While α, β and δ rotors had very similar thermal rotational onset temperatures, Figure 6.5 reveals that δ-rotors have distinctly different rotational energetics. α and β rotors still appear to have almost identical rotational properties (within error), but upon examination of their rotational rates it is clear that δ-adsorbed species have very different rotational rates at lower temperatures and have a lower activation energy. γ rotor species spin so quickly even at 5 K that it is not possible to measure their rotational rates due to the time resolution of the *I* vs. *t* curves (1-3 kHz for our setup depending on tunneling current set-point).[91] Figure 6.5 reveals the marked difference in rotational rates

for the same molecules at the same measurement conditions and the same temperature, with the only difference between them being their adsorption sites.

The activation energies (E_a) and the attempt frequencies (A) calculated from the Arrhenius plots are displayed in Table 6.1. The attempt frequencies are noticeably low compared to expected molecular event frequencies; however, this low attempt frequency has been observed previously for single molecule rotors, including this group's work of similar molecular rotors. It has been postulated that the low A values arise due to multiple configurations of the alkyl tails in the ground state that lead to entropic effects in the transition state or tunneling effects.[37,95-97,119] Although it is not possible to plot Arrhenius data for the γ rotors, a barrier was estimated for comparison to other adsorbed rotor species. In this calculation the minimum rate was used (estimated based on experimental limitations) and 10^8 Hz was used as an attempt frequency (based on all of the other adsorbed species). It is expected that this is an overestimation of the activation energy for the γ rotors, however, it emphasizes the differences in rotational properties between these rotor molecules based solely on their different adsorption sites.

Table 6.1: Arrhenius data for α, β and δ adsorption sites. All italicized numbers are estimated. [1]γ rotors spin too quickly to measure rotational rates experimentally even at 5 K, therefore it was not possible to take rate measurements for this adsorption site; however, using the minimum rate based on experimental limitations an upper limit for the barrier was estimated for comparison to other adsorbed rotor species. [2]Adsorption energies are estimated based on an interpolated value for the equilibrated species and a common ratio between adsorption energy and rotational barrier. [3]While α and β have the same rotational rate within error, an experimentally-measured Boltzmann distribution at 45 K shows that there is a 2 kJ/mol difference between these species. Errors are reported to 1 standard deviation.

	E_a (kJ/mol)	A (Hz)	ΔE_{ads}[2] (kJ/mol)
α	0.9 ± 0.1	$9 \times 10^{7 \pm 0.9}$	*-78 ± 8*
β	0.9 ± 0.1	$2 \times 10^{8 \pm 1}$	*-76 ± 8*[3]
γ	*≤0.2*[1]	--	*-17 ± 2*
δ	0.6 ± 0.1	$1 \times 10^{9 \pm 1}$	*-52 ± 5*

It is well known that there is an approximately linear relationship between adsorption energy and barrier to diffusion[120-122]; therefore, we propose that there exists a similar correlation between adsorption energy and barrier to rotation. Molecular Dynamics simulations have shown that there is a delicate interplay between S-Au bond length, alkyl tail length and rotational dynamics of thioether molecules, which suggests that the S-Au bond strength is strongly coupled to the rotational properties of similar molecular species.[62] Previous studies by Lavrich *et al.* used temperature programmed desorption (TPD) to find the desorption energies for a range of alkane thiol and thioether molecules[53]. Lavrich and coworkers reported desorption energies for dibutyl sulfide and diethyl sulfide of 86 and 68 kJ/mol, respectively[53]. We have previously studied the rotation of symmetric thioethers, including both dibutyl and diethyl sulfides[37] and have found their barriers to rotation to be 1.2 ± 0.1 and 0.65 ± 0.06 kJ/mol,

respectively. Both of these molecules give a ratio of desorption energy to rotational barrier of ~0.01. This ratio, coupled with the knowledge that the equilibrated butyl methyl sulfide rotors have a rotational barrier of 0.9 kJ/mol, leads to an interpolated desorption energy for butyl methyl sulfide of 78 ± 8 kJ/mol. From this value for the most stable rotors (α) and the ratios of the rotational barriers to that of the α species, adsorption energies were calculated for the three metastable species (see Table 6.1). α and β were measured to have the same rotational rates within error, but from equilibration data like that shown in Figure 6.3, it is clear that the α molecules are in lower energy sites than the β species. The energetic difference between these species was then calculated using a Boltzmann distribution at 45 K, which yields a 2 kJ/mol difference between these two species.

Using the experimentally-measured temperatures at which the metastable rotors equilibrated (Figure 6.3) it was possible to calculate the energetic barriers to transition between adsorption sites (i.e. diffusion barriers). For these calculations an equilibration rate of 1 event every 1,000 seconds was estimated from experimental data, and an attempt frequency of 10^{12} Hz was assumed (which is an average attempt frequency for diffusion of molecular species)[120]. Using all the calculated diffusion barriers and adsorption energies it is possible to create an energetic landscape for all adsorbed species, which is shown in Figure 6.6. It is interesting to note that the more stable adsorption sites have

higher diffusion barriers for moving to the equilibration site, while less stable sites have lower barriers ($\gamma < \delta < \beta$). This makes sense based on transition state theory, which predicts that the more stable the initial state, the higher the barrier for transitioning to a stable final state.[123]

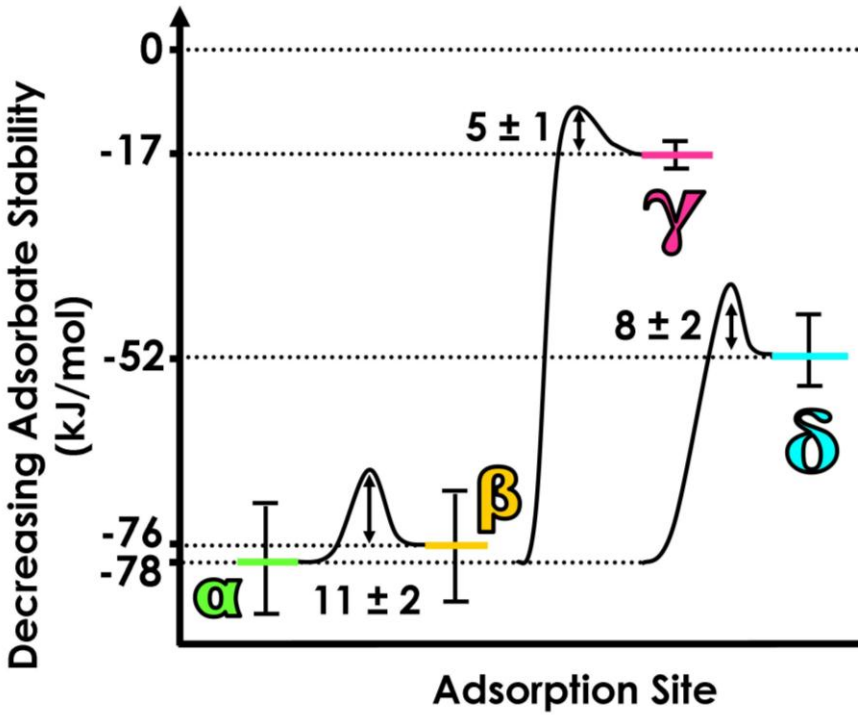

Figure 6.6: Proposed energy diagram for butyl methyl sulfide adsorbed at different sites on Au(111). Energies are shown in kJ/mol for both adsorption energies and barriers to diffusion to the most stable adsorption site.

Based on the rotational energetics data and the appearance upon STM imaging we can propose adsorption sites for the three metastable species. Figure 6.7 shows 3D renderings of high-resolution STM images for molecules in each of the four adsorption sites using the same STM tip state, where it can be seen that

the adsorption site difference leads to dramatically different appearances. Images such as those in Figure 6.7 help provide insight into the adsorption site of each molecule. Based on previous DFT studies[91,119] we know that the most stable (α) species adsorbs nearly atop a Au atom and rotates off axis with the S atom precessing as the alkyl tails rotate. This leads to the chiral pinwheel appearance of the molecules.[119] It is unlikely that atop and off atop sites (which are <0.05nm apart) would have extremely different adsorption energies. By this argument we postulate that β rotors adsorb directly atop, with an adsorption energy very similar to that of the α adsorption sites. This hypothesis is supported by the appearance of β rotors in STM images. β rotors appear hexagonal and do not appear to possess chirality (as evidenced by the pinwheel appearance of the α rotors), as would be expected for a high symmetry site like atop adsorption. δ rotors are postulated to adsorb on a bridge site, which is supported by their two distinct sets of three lobes seen in STM imaging. Adsorption at a bridge site would be expected to lead to such a mirror plane being imposed on the six-fold symmetry of the rotating molecule. Finally, γ rotors are proposed to be in the remaining sites, the three-fold hollows, with less favorable adsorption energies and lower barriers to diffusion and rotation. Again, three fold hollow sites have high symmetry as supported by the hexagonal appearance of the γ rotors.

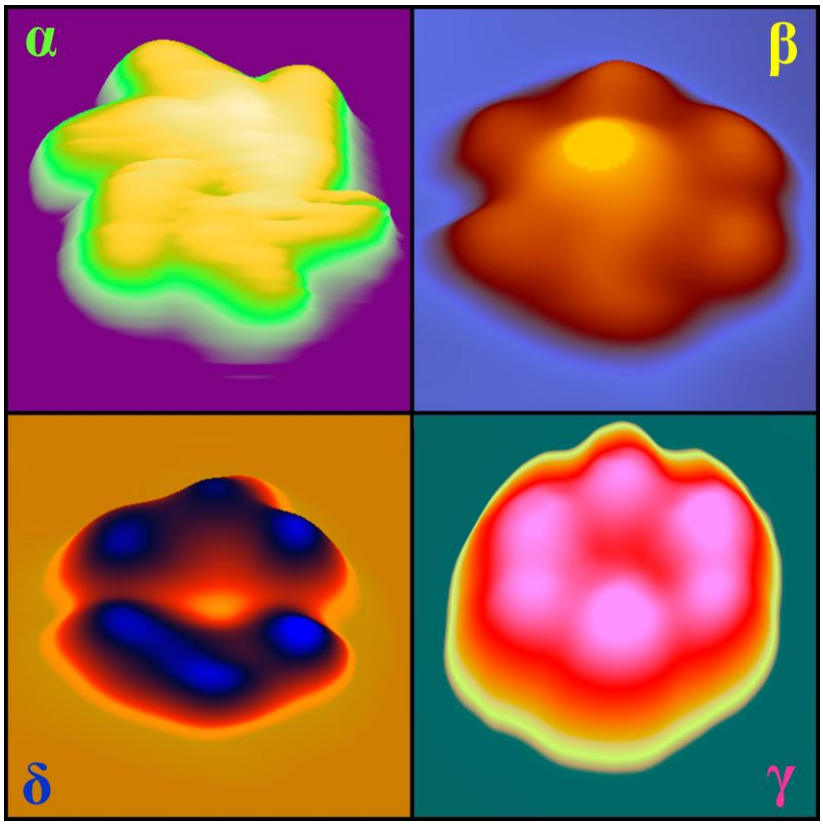

Figure 6.7: 3D rendering of high-resolution STM images provide information on the symmetry of the rotating molecule's environment and insight for the assignment of each adsorption site. All four images were recorded with the same tip state.

Percentages of molecules in each of the sites were both calculated based on these assignments and quantified from experimental data for a population of >100 molecules (Table 6.1). The classical adsorption sites are atop, bridge, and three-fold hollows, which occur in a ratio of 1:3:2 (Figure 6.8). This ratio does not account for the off-atop sites which were found to be the energetic minimum for the equilibrated rotor species using DFT.[119] The classical sites are typically the only ones considered, as it usually assumed that if a molecule is close to a classical adsorption site, it can relax into the lowest energy site. However, in our

system we are working with a surface at 5 K and a molecule that does not posses the energy needed to diffuse even a fraction of a nanometer, so this adsorption site area, or "footprint", becomes important. By calculating an approximate area for the off-atop "ring" shown in Figure 6.8 (and knowing the approximate radius of this ring from previous DFT calculations[119]) it is found that the relative areas presented are ~ 1:1 for bridge sites and the off atop ring based on their approximate sizes. Random, as-dosed populations were then estimated using these adsorption site surface area ratios (as shown in Table 6.2) which match well with the experimentally measured as-dosed populations of the sites. The estimated populations should be viewed with caution, as an incoming molecule does not encounter a ratio of possible sites, but only senses the potential energy landscape at the point of its impact. With this in mind, there appears to be a relatively strong correlation with the experimental data, which suggests that this ratio of possible sites may be a simple descriptor for a very complex phenomenon. While in-depth DFT studies may provide further insight into the exact sites of adsorption for these species, these studies would not be trivial as local minima sites are found in abundance for any potential energy surface. While this study does not necessarily yield definitive evidence for the exact assignment of each of the three non-equilibrium adsorption sites of butyl methyl sulfide, absolute assignment of these sites is not needed to appreciate the distinct

differences in physical properties exhibited by the same molecule in each of these four different adsorption sites.

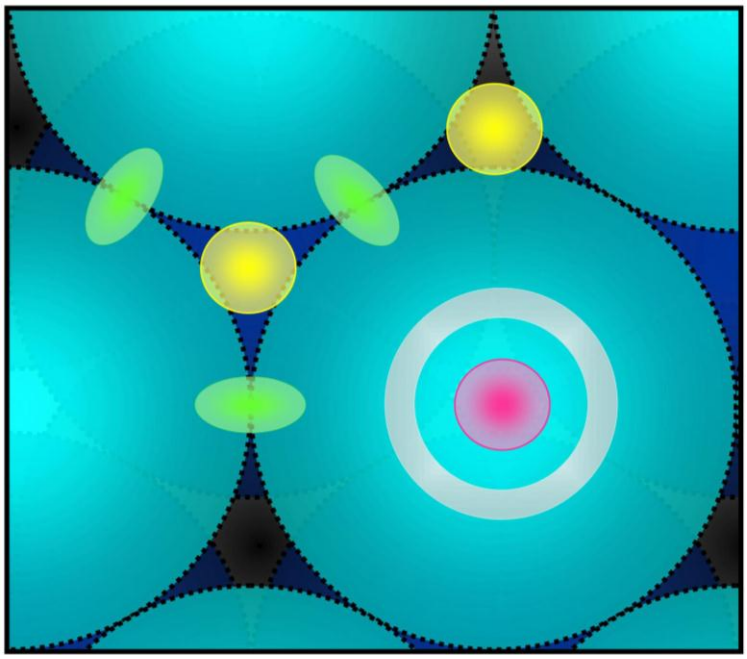

Figure 6.8: Schematic of available adsorption sites for incoming species. The classical adsorption sites are shown in their abundance ratio of 1:3:2 for atop (pink), bridge (green), and three-fold hollows (yellow). Atoms in the surface are shown as light blue, dark blue and black for the 1st, 2nd and 3rd layers, respectively. A ring is also shown in white for the off atop adsorption, which is the equilibrium site for butyl methyl sulfide molecules predicted by DFT.[119]

Table 6.2: A comparison of the simplistic, estimated population based on the ratio of possible adsorption sites and the experimentally-measured data for as-deposited molecules at 5 K. Off atop sites are estimated based on their available surface area for adsorption.

	Proposed site	**Estimated population**	**Actual population**
α	off atop	33%	38%
β	atop	11%	12%
γ	3-fold	22%	17%
δ	bridge	33%	33%

6.4 Conclusions

Low-temperature STM has been used to elucidate details of the adsorption of a simple thioether molecule (butyl methyl sulfide) on a Au(111) surface. Interestingly, when adsorbed at 5 K these molecules did not have sufficient energy to reach their equilibrium adsorption sites, and existed in four distinct adsorption sites on the surface. Molecular adsorption in these non-equilibrium sites was shown to lead to markedly different appearances of the molecules in STM imaging and very different rotational energetics. Equilibration of each of the non-equilibrium (or precursor) species was studied as a function of bias voltage and temperature, and it was observed that the vast majority of the molecules eventually diffused to their equilibrium site, the properties of which had been studied previously using STM and DFT. From experimental measurements a relationship was proposed between the adsorption energy and the barrier to rotation, somewhat analogous to well known corrugation ratios which relate adsorption energy to diffusion barrier.[121,122] It was found that molecules in more stable adsorption sites had higher barriers to diffuse to their equilibrium adsorption sites, which would be expected from transition state theory.[123] This work illustrates the distinctly different physical properties exhibited by molecules in different adsorption sites and emphasizes the need for an understanding of the atomic-scale details of adsorption sites and the behavior of non-equilibrium molecular species. While it is true that surface assemblies and

reactions involve mainly equilibrated species, it is often the case that some proportion of the ensemble is adsorbed at non-equilibrium sites. Even if this number is small, the differences in adsorption site energy and barriers to motion which we report here may lead to reactivity of the minority that overwhelms the majority and dominates the ensemble properties.

Chapter 7

Regular Scanning Tunneling Microscope Tips can be Intrinsically Chiral

7.1 Introduction

From the question of the origin of homochiral life to enantioselective drug production, the study of chirality is ubiquitous in science. Over the last decade, pioneering scanning probe studies have revealed that chiral recognition, separation, amplification, and transfer into supramolecular structures can all be tracked and understood at the single-molecule level.[85,124-137] Furthermore, theory has been used to predict many novel interactions between chiral molecules and electrons.[138-140] Herein we report the discovery that regular scanning tunneling microscope tips can themselves be chiral. This chirality leads to different electron tunneling efficiencies through left-handed and right-handed molecules. The effect manifests itself as small topographic height differences between the two chiralities. When using the tip to electrically excite molecular rotation, large differences in the rate of molecular rotation were observed that correlated with each individual molecule's chirality. While this work has major consequences for the study of two-dimensional chiral systems[82,85,124-128,130,132,134,141], more importantly it offers a new method for interrogating the effect of chirality on electron transport in a controlled manner, on a molecule-by-molecule basis.

7.2 Experimental Methods

Butyl methyl sulfide (BuSMe) was obtained from Sigma Aldrich and further purified by cycles of freeze/pump/thaw prior to introduction to the STM via a leak valve. The final purity of BuSMe was verified by mass spectra and STM imaging to be >98%. All data was recorded for molecules >10 nm from a step edge to exclude any effects that may arise from kinks or steps.

7.3 Results and Discussion

When adsorbed on the terrace of a (111) facet of a metal surface, thioethers rotate around the central sulfur-metal bond and appear hexagonal in shape due to the threefold symmetry of the underlying surface (Figure 7.1a).[37,90,119] BuSMe is achiral in the gas phase but, due to its asymmetry, has two prochiral lone pairs on the central S atom that give rise to chirality in the surface-bound molecules (see Figure 7.1b for a schematic).[68,94,119] Since binding to a surface occurs through one of the lone pairs on the sulfur atom and that the alkyl tails lie almost parallel to the surface.[119] The unbonded lone pair remains unperturbed and the geometry around the S atom is essentially tetrahedral; hence, R and S enantiomers of the prochiral molecule are formed with an inversion barrier between enantiomers that is calculated to be 0.24 eV. The rapidly rotating molecules can be clearly distinguished upon atomic-scale imaging by their mirror image pinwheel appearance[119] (as seen in Figure 7.1a) which arises from an off-center precession

of the central S atom around the top of a surface atom with a precession diameter of 0.1 nm.[119]

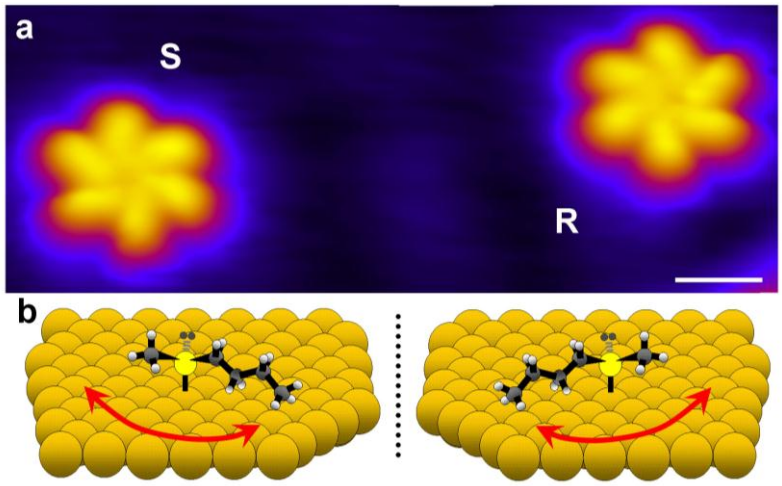

Figure 7.1: Single molecule chiral identification. a) STM image of the two enantiomeric, mirror image forms (R and S) of BuSMe adsorbed on Cu(111). The pinwheel appearance of the molecule arises from the fast rotation of the alkyl groups around the central S atom. b) Schematic showing that while BuSMe is achiral in the gas phase, adsorption on a surface results in two enantiomers depending on which of the prochiral lone pairs bonds to the surface.[119] (Imaging conditions: I = 300 pA, V = 100 mV, T = 7 K. Scale bar = 1 nm).

Just as one's right and left hands should have the same dimensions, one would expect the R and S enantiomers of surface-bound BuSMe to have the same widths and heights. Interestingly, careful measurements of the topographic heights of R and S molecules from STM images revealed that, in any given experiment, either the R or S enantiomers would appear topographically higher. While any particular STM tip yielded reproducible height differences between the enantiomers, alteration of the tip state led to a different height difference. Changes in the tip state were produced in the form of minor alterations via

voltage pulses (4-10 V) or surface indentations (~0.1-1 nm), or as major changes such as substitution of an entirely new tip. Figure 7.2a shows height difference data from ten representative STM tips revealing that, even with the relativity large error bars associated with such small height differences, either of the two enantiomers can appear higher with a given tip state and that some tips yield no discernable height difference. As the topographic heights of two enantiomers (R and S) measured with an achiral probe on an achiral surface must be the same, the only explanation for these results is that regular STM tips themselves can be chiral. Figure 7.2b shows a schematic in which the three atoms of the STM tip closest to the surface are colored, and a proposed tip trajectory for a chiral tip. Providing the last three or more atoms are at different heights above the surface, the three-point contact model predicts that a diastereomeric relationship exists between a surface-bound enantiomer and the tip. This diastereomeric interaction can lead to different electron tunneling efficiencies, and therefore topographic height differences. Just as bare metal surfaces can possess chirality due to the arrangement of atoms at kink sites[142,143] and metal nanoparticles can adopt chiral structures[144], we propose that bare metal STM tips can be chiral based on the arrangement of the atoms at the end of the tip.

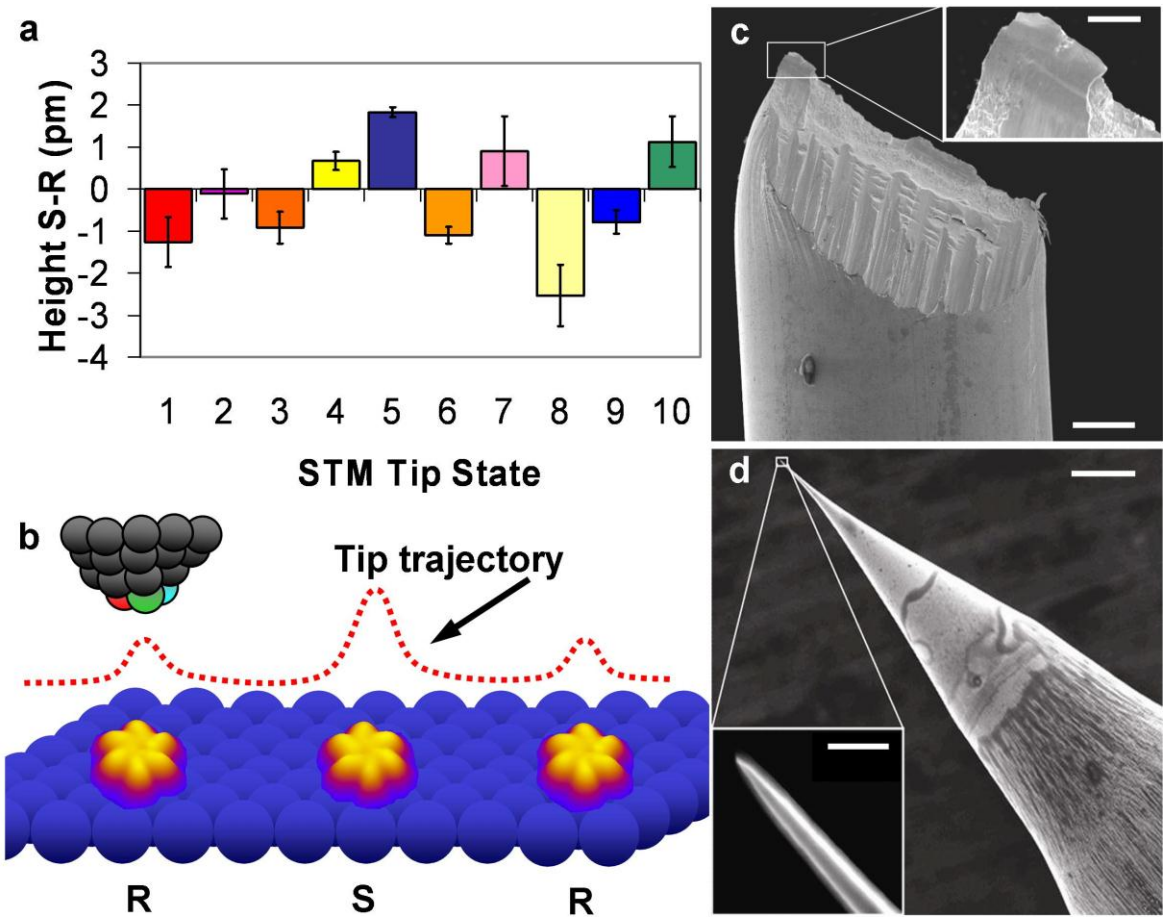

Figure 7.2: a) Graph of height difference between the R and S enantiomers of BuSMe on Cu(111) measured with ten different STM tip states revealing that regular STM tips can be intrinsically chiral. Height measurements for each tip state are taken for populations of >50 molecules. Error bars are reported to 1 standard deviation. b) Schematic showing that if the last three or more atoms on the STM tip are different heights above the surface, then the three point contact model leads to a diastereomeric relationship, different tunneling efficiencies, and the ability to differentiate between enantiomers based on their topographic height. c) SEM images of a cut Pt/Ir STM tip. Scale bar = 50 µm, inset = 10 µm. d) SEM images of an etched W STM tip. Scale bar = 50 µm, inset = 0.5 µm.

Figures 7.2c and 7.2d show scanning electron microscope (SEM) images of regular Pt/Ir and W STM tips. From these images it is apparent, especially for the cut Pt/Ir tip, that even at the microscopic level (>1000x the size of atoms) the tip is an asymmetric entity. While atomic resolution is beyond the limit of SEMs,

it is not unreasonable to expect that if more than one atom from the tip contributes to the tunneling current, as long as these atoms are not in a completely symmetrical geometric arrangement, the tunneling portion of the STM tip will be chiral.

This result is initially surprising given that the STM tip is normally considered to be a point source of electrons. However, well-known image artifacts arising from what are commonly referred to as "double" or "triple tips" are direct evidence for tunneling through more than one point. Our discovery indicates that a much more subtle version of this effect is also at play and only manifests itself when studying chiral molecules with very high spatial resolution.

As further evidence for this phenomenon a second set of experiments was conducted in which the rate of electrically-driven rotation of R and S enantiomers was measured with the same STM tip. If the STM tip was achiral one would expect identical rates of rotation of R and S rotors for the same excitation conditions. The rotation of the molecules was both driven and measured by the electron tunneling current, and for each STM tip between 10^3 and 10^5 molecular rotational events were recorded and quantified, and a rotation rate was calculated. Our previous work has shown that this electrically-excited rotation is driven by electrons of energy > 0.37 eV via excitation of a C-H vibration that in turn couples selectively to the rotation of the molecule.[90]

Table 7.1 Rotational rate (Hz) for each enantiomer as a function of STM tip state. All rate data is taken at identical tunneling conditions: 380 mV, 5 pA. Error bars are reported to 1 standard deviation.

Tip State	A	B	C	D
R enantiomer	30 ±10	50 ±20	30 ±10	63 ±9
S enantiomer	70 ±20	82 ±9	25 ±7	40 ±10

Table 7.1 shows rotational rates for the R and S rotor enantiomers acquired using four different tip states. Extreme care was taken to ensure that the tip state remained unchanged for the duration of each experiment. Any STM tip changes during the measurement were readily observed as changes in the baseline tunneling current during electrical excitation. Immediately apparent from Table 7.1 is that the rotational rate is highly tip state dependent. All of these rate measurements were made using the same tunneling current and voltage; therefore, the overall rotational rate differences from tip state to tip state must be due to differences in the inelastic electron tunneling efficiency of the tips. This effect of variations in coupling efficiencies for different STM tips has been observed previously when exciting vibrational or rotational motions.[145] Next, and most importantly, it is apparent that for a given tip state one of the enantiomers spins more quickly than the other. Just as with the height difference data, the only way to explain how identical electrical excitation of two surface-bound enantiomers can lead to different physical rates is via a diastereomeric interaction with a chiral entity, i.e. the STM tip.

7.4 Conclusions

It is initially somewhat surprising that in the ~30 years since STM was invented it has never been reported that regular STM tips can be intrinsically chiral. However, this quandary can be rationalized by the fact that the magnitude of the effect in a normal topographic imaging mode (1-2 pm) is below the detection limit of most instruments (typically >5 pm). These results have great significance for all surface studies of chirality given that the role of the scanning probe tip is often considered as merely a spectator. The fact that single enantiomers can be distinguished based solely on height measurements from a topographic image without functionalizing the tip yields a new method for chirality to be identified for a set of surface-bound enantiomers in a single-molecule version of Pasteur's famous experiment. As the BuSMe molecule's chirality can be gleaned from its pinwheel appearance, it may be a useful "chirality standard" by which a STM tip's chirality can be assessed via height measurements. Of equal or potentially more importance is the result that this subtle tip chirality, not measurable by most STM instruments, can have a large effect on the dynamics of a probed chiral molecule. We have demonstrated that the diasteromerism arising from the interaction of a chiral tip and a molecule can lead to large differences in inelastic electron-induced dynamics of the enantiomers. This is another important consideration in the study of chiral surface systems and potentially offers a novel way to study enantiospecific

interactions and the effect of chirality on electron transport at the single-molecule level.

Chapter 8

Electrically-Driven Motion of a Single-Molecule Rotary Motor

8.1 Introduction

Molecular motors are prevalent in nature in the form of motor proteins[1-4], yet limited progress has been made toward creating synthetic motors.[5,6,146] In order to create a nanoscale motor, the mechanical components must be able to convert incoming energy into directed and controllable motion.[147] Great strides have been made by creating chemically-driven linear motors[148], and optically-driven rotary motors;[149] however, little progress has been made in using electrical energy to direct motion.[150] Here we show the first progress in creating an electrically-driven single-molecule motor. By providing electrical energy via a STM tip, 5% directed rotation can be achieved. While 5% directed rotation is nowhere near fully-unidirectional motion, this is a large step toward the creation of useful nanomachines. 5% unidirectionality at a rate of 10^1-10^2 Hz leads to full, unidirectional rotations on the order of once every few seconds, and using electrically energy it is possible to interrogate small groups of molecules or even a single molecule at a time.

8.2 Experimental Methods

Butyl methyl sulfide (BuSMe) was obtained from Sigma Aldrich and further purified by cycles of freeze/pump/thaw prior to introduction to the STM via a leak valve. The final purity of BuSMe was verified by mass spectra and STM imaging to be >98%.

8.3 Results and Discussion

BuSMe is achiral in the gas phase but, due to its asymmetry, has two prochiral lone pairs on the central S atom that give rise to chirality in the surface-bound molecules. The STM image in Figure 8.1 reveals that the two enantiomers of BuSMe appear as pinwheels related by mirror symmetry.[151] The left-handed and right-handed pinwheels are named here by the Cahn-Ingold-Prelog rules as "R" and "S".[152]

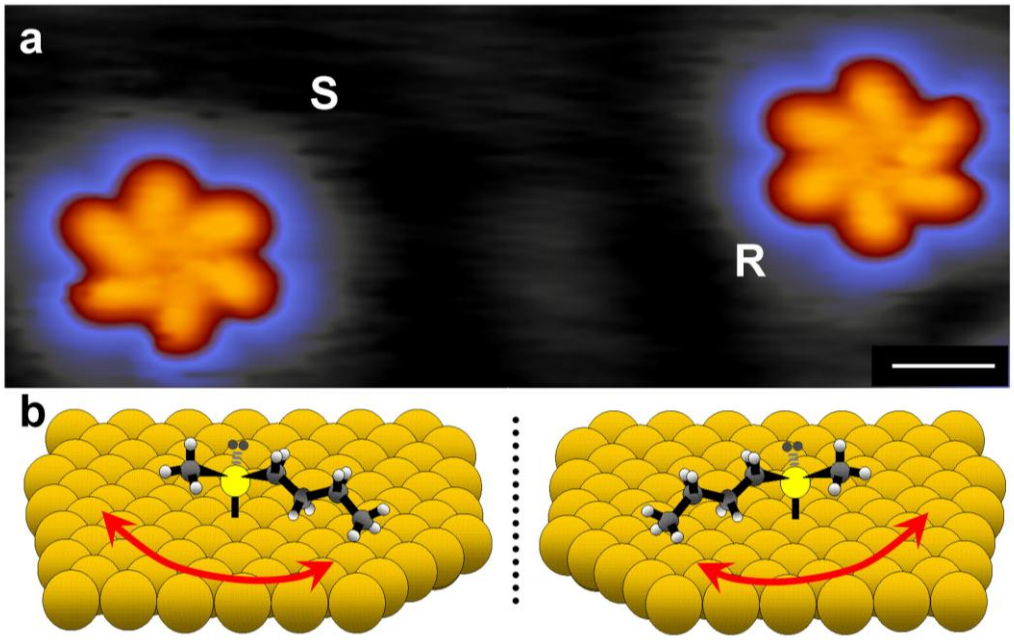

Figure 8.1: Single molecule rotors (A) STM image of the two enantiomeric forms of BuSMe adsorbed on Cu(111). The pinwheel appearance of the molecule arises from the fast rotation of the alkyl groups around the central S atom. (B) Schematic showing that while BuSMe is achiral in the gas phase, adsorption on a surface results in two enantiomers depending on which of the prochiral lone pairs bonds to the surface. (Imaging Conditions: I = 300 pA, Vtip = 100 mV, T = 7 K, scale bar = 0.5 nm).

Using STM it is possible to measure the rotational rates and even the directionality of rotation for these molecules, as described in section 1.2. Figure 8.2 shows a *I* vs. *t* curve taken during the electrical excitation of a BuSMe molecule. All six states are visible, each of which corresponds to one of the six possible positions of the alkyl tails within the molecular rotational cycle.[119]

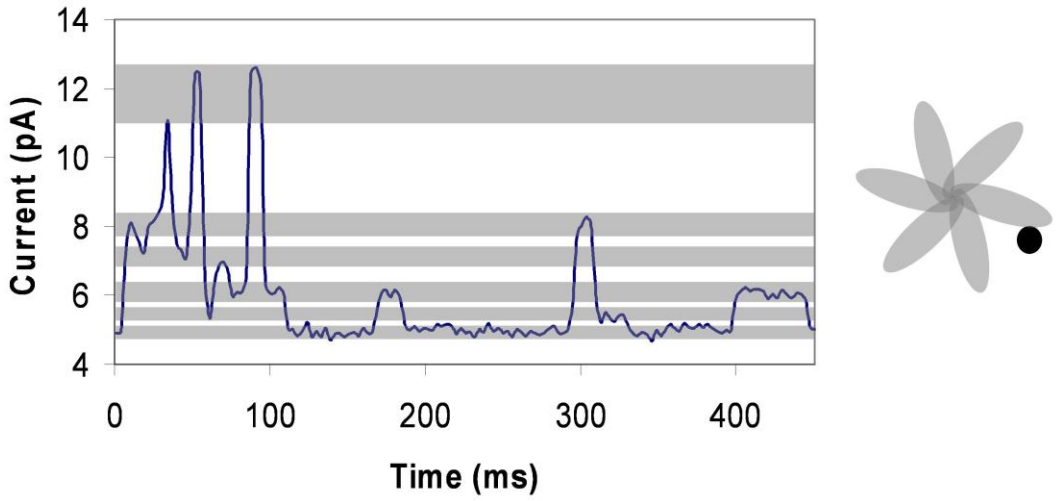

Figure 8.2: Measuring rotational rate and directionality I vs. t curves provide a way to measure both rotational rate (events/time) as well as the directionality of rotation by following the progression of the molecule between its six possible states. Schematic on the right shows these six states, as well as the tip position (black circle) which would create inequivalent current levels for each state. Curve conditions: 5 pA, 380 mV.

In order to create a useful rotary motor, the rotation must be a directed motion, meaning that the molecule rotates more clockwise than anticlockwise (or vice versa). Using our *I* vs. *t* measurements, we have measured the directionality of rotating molecules as a function of molecular identity and energy sources. The rotation of the molecules was driven thermally or electrically, and measured by the electron tunneling current using a method described previously.[90] Our previous work has shown that the electrically-excited rotation is driven by electrons of energy > 0.37 eV via excitation of a C-H vibration, which couples selectively to the rotation of the molecule.[90] For each STM tip between 10^3 and 10^5 molecular rotational events were recorded and quantified, and both rotation rate and directionality were calculated.

Table 8.1 shows directionality measured for symmetric dibutyl sulfide molecules as well as the asymmetric BuSMe molecule. Thermal and electrical energy sources are shown, and it can be seen that no directionality was achieved using thermal energy, as would be predicted by the 2nd law of thermodynamics. Only by using electrical energy with the asymmetric torsional potential of the asymmetric molecule was directionality achieved.

Table 8.1: Effects of molecular identity and energy source on directed rotation. Measured directionality is shown for dibutyl sulfide and butyl methyl sulfide using thermal or electrical energy to fuel rotation

Molecule	**Energy Source**	**Directionality**
Dibutyl Sulfide	Heat	0 ± 1 %
(R)-Butyl Methyl Sulfide	Heat	0 ± 2 %
(R)-Butyl Methyl Sulfide	Electrical	5.2 ± 0.8 %
(S)-Butyl Methyl Sulfide	Electrical	1.4 ± 0.4 %

Interestingly, this directionality was seen more prevalently for one of the two surface-bound enantiomers of BuSMe. The other enantiomer, which is identical in the gas-phase and should have identical properties when attached to a surface, only showed around 1% directionality. Our group has recently shown that even bare metal STM tips can be intrinsically chiral.[153] Using this intrinsic chirality to interact with the surface-bound enantiomers, a diastereomeric relationship arises between the tip and the molecule. A three-point contact model[154] suggests that only three atoms in the STM tip need to contribute to the tunneling current to create this diastereomeric relationship. Due to this

asymmetry of the probe, the tip will interact differently with one surface-bound enantiomer than the other (Figure 8.3). Figure 8.3 shows a simplistic diagram of a chiral probe (the STM tip) interacting with two surface-bound enantiomers. The tip itself does not have a torsional potential, but instead imposes a chiral potential onto the rotating enantiomers.

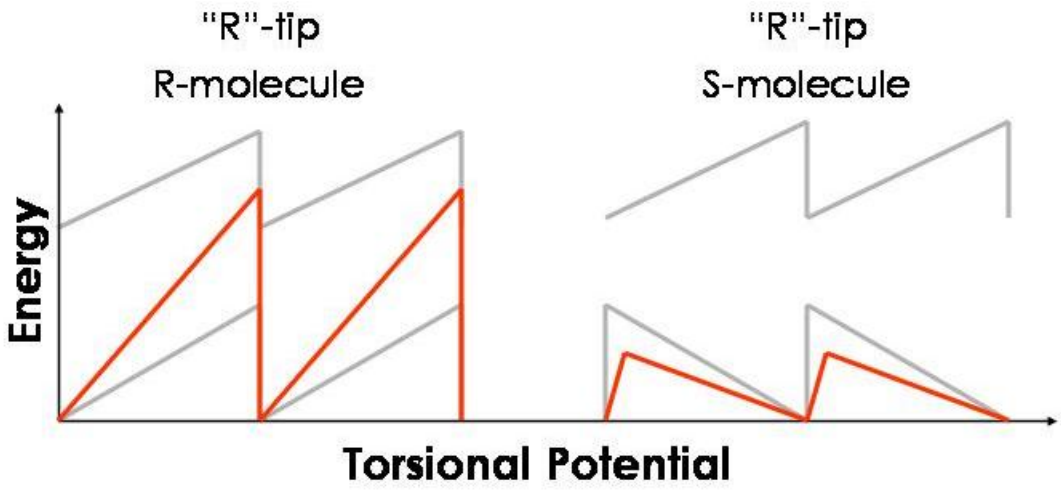

Figure 8.3: Simplistic diagram of interaction of a chiral probe with the two surface-bound enantiomers. A chiral probe imposes a chiral potential onto the molecule being scanned, leading to a diastereomeric interaction between the tip and surface. Grayed lines show potentials for the tip (top) and molecule (bottom). The red lines show total torsional potentials for each of molecule-tip interactions.

We have shown previously that this diastereomeric relationship causes dramatic differences in rotational rate between the surface-bound enantiomers of BuSMe.[153] We believe that it is this diasteriomerism that also leads to the difference in directionality for the two enantiomers. Table 8.2 shows how the degree of directionality changes as a function of tip state. Depending on the

interaction of the tip with the two enantiomers, either the R or S molecules will rotate with more directionality; however the opposite enantiomer will rotate more quickly. As an "R" tip may interact more strongly with an R molecule, this would lead to a higher, but more asymmetric torsional potential, leading to slower, but more directional motion. The S enantiomer on the other hand would have a smaller, but more symmetric rotational potential, and would thus spin more quickly, but with less directionality (Figure 8.3). Table 8.2 shows this trend for multiple tip states, and it is seen that some tip states are achiral, and do not provide directionality or any difference in rotation rate.

Table 8.2: Tip state effects on rotational rate and directionality. Both rate and directionality were measured as a function of tip state for the R and S surface-bound enantiomers of butyl methyl sulfide. It can be seen that both rate and directionality are highly tip state dependent.

	Directionality (%)		Rate (Hz)	
	R	S	R	S
Tip State 1	5.2 ± 0.8	1.4 ± 0.4	29 ± 5	70 ± 10
Tip State 2	5 ± 1	1 ± 1	30 ± 10	50 ± 30
Tip State 3	0 ± 2	0 ± 2	15 ± 5	14 ± 3

8.4 Conclusions

While 5% directed rotation is nowhere near fully-unidirectional motion, this is a large step toward the creation of useful nanomachines. Even with only 5% unidirectionality at a rate of 10^1-10^2 Hz, this leads to full, unidirectional rotations on the order of once every few seconds. Many chemically-driven

molecular motors can take hours or even days to achieve a complete directional cycle.[148] On the other hand, optically-driven rotation has been shown to provide directional motion at rates up to 10^6 Hz;[149] however, optical means of driving motion are not very selective. Due to the wavelength of light in comparison to the size of molecules, even with the finest radiation sources hundreds or thousands of molecules are being irradiated at the same time. Using electrical sources it is possible to excite small populations of molecules, or even just a single molecule at a time.

Chapter 9

Symmetry Breaking at the Single-Molecule Limit

9.1 Introduction

Ever since Pasteur used tweezers to manually separate enantiopure crystals of sodium ammonium tartrate[155], the idea of chirality has fascinated scientists[82,85,124-128,130,133,141,156]. Industrially, the selective conversion of prochiral reagents to chiral products is a crucial step in the production of a variety of asymmetric pharmaceuticals. While this feat is accomplished using either chiral catalysts or crystallization, many external influences have been shown to be capable of inducing such symmetry breaking including circularly polarized light[157-159], spin-polarized electrons[160], and combinations of unpolarized light and magnetic fields[161]. Pioneering studies have made great strides towards explaining these various interactions; however many of the fundamental mechanisms by which chirality is transferred at the molecular-level are not yet fully understood. It is also a great challenge to design experimental setups with which to study these phenomena in a quantitative and reproducible manner[157].

Herein we describe a system consisting of prochiral molecules adsorbed on an achiral surface in which enantiomeric excesses of the chiral adsorbed state of the molecule can be quantified at the single-molecule level in a clean and well-defined environment. We find that while thermal equilibration yields racemic

mixtures, electrical excitation results in a surprisingly large symmetry breaking effect.

9.2 Experimental Details

Butyl methyl sulfide (BuSMe) was obtained from Sigma Aldrich and further purified by cycles of freeze/pump/thaw prior to introduction to the STM via a leak valve. The final purity of BuSMe was verified by mass spectra and STM imaging to be >98%.

9.3 Results and Discussion

Butyl methyl sulfide (BuSMe) appears hexagonal in shape due to its rotation abovea hexagonally symmetric underlying surface.[37,90,119] The six equivalent time-averaged orientations of the butyl tail lead to BuSMe's pinwheel appearance in STM images.[119] Similar pinwheel shaped molecules have been reported previously due to an off-center rotation of the rotor's axle.[12,119] BuSMe is achiral in the gas phase but, due to its asymmetry, has two prochiral lone pairs on the central S atom that give rise to chirality in the surface-bound molecules. Figure 9.1 reveals that the two enantiomers of BuSMe are visually distinct in the STM images, i.e. the rotor pinwheels are non-superimposable but related by mirror symmetry. All individual BuSMe molecules appeared in STM images as

either left- or right-handed (R or S) pinwheels when adsorbed in their equilibrium adsorption sites.[119]

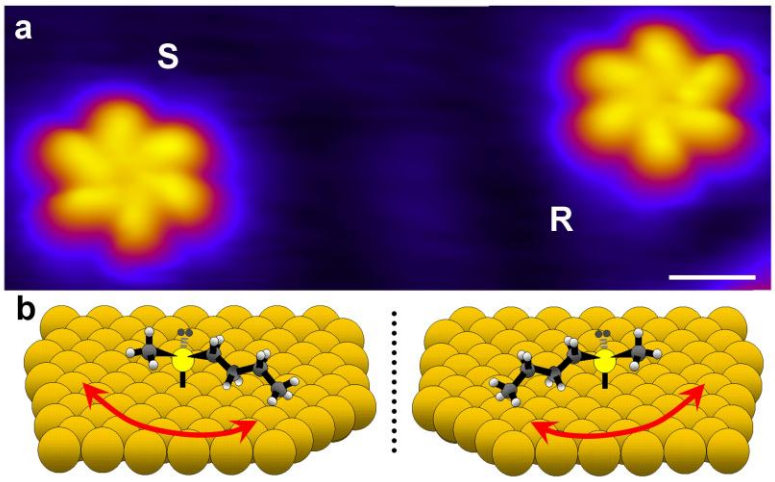

Figure 9.1: Chiral identification of single molecules. a) STM image of the two enantiomeric forms (denoted R and S) of BuSMe adsorbed on Cu(111). The pinwheel appearance of the molecule arises from the fast rotation of the alkyl groups around the central S atom. b) Schematic showing that while BuSMe is achiral in the gas phase, adsorption on a surface results in two enantiomers depending on which of the prochiral lone pairs bonds to the surface. (Imaging Conditions: I = 300 pA, V = 100 mV, T = 7 K, scale bar = 0.5 nm).

When BuSMe was deposited on the Cu(111) surface at 7 K the molecules did not have sufficient energy to reach their equilibrium adsorption sites and appeared in STM images as irregularly shaped protrusions that were fairly mobile (Figure 9.2a). Such intrinsic precursors to chemisorption are well known and have previously been isolated for the case of benzene on Si(111)[114]. Wolkow and co-workers found that benzene adsorbed on Si(111) below 80 K occupied a mobile physisorbed state that could be transformed to the chemisorbed state by

heating the Si(111) surface to 95 K. We found that the metastable BuSMe molecules could be transitioned to their equilibrium adsorption sites by either thermal annealing to 80 K or by applying a voltage pulse from the STM tip. Figure 9.2 shows that applying 400 mV pulses directly above the four imaged molecules caused them to change from the precursor state to the familiar pinwheel state associated with their preferred adsorption site. It has been shown that thermal annealing or electrical excitation transition all precursor BuSMe molecules into their equilibrium adsorption sites.[162]

Surprisingly, when voltage pulses were applied to sets of molecules, the expected 50:50 ratios of R and S enantiomers were not observed. Eleven different tips were used to pulse sets of ~50 molecules and enantiomeric excesses (*ee*'s) of up to 39±5 % were observed. By comparison, the thermal control experiments always yielded near 50:50 mixes of the enantiomers with typical *ee*'s no higher than 3 ±6 %. The error bars for all *ee's* are quoted ± 1 standard deviation.

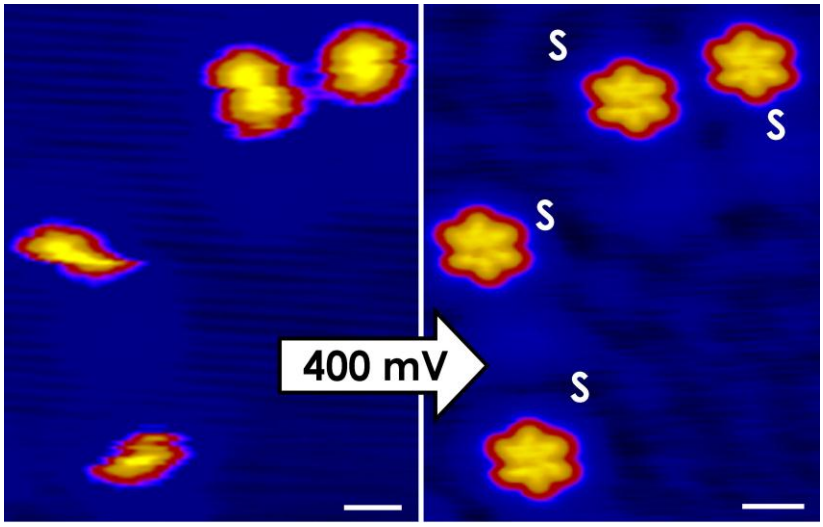

Figure 9.2: Electrical excitation of prochiral molecules in precursor states leads to symmetry breaking. Left: STM image of four BuSMe molecules in a weakly-bound precursor state on Cu(111) at 7 K. Right: STM image of the same four molecules after electrical excitation by the STM tip caused them to move to their preferred adsorption sites in which they are more strongly bound and their fast rotation leads to their pinwheel appearance. (Imaging Conditions left: I = 10 pA, V = 100 mV, T = 7 K, right: I = 300 pA, V = 100 mV, T = 7 K). Scale bars = 1 nm.

This dramatic departure from the expected racemic mixture is very surprising because the Cu(111) surface is achiral and the molecules are prochiral. Given that these experiments were performed under ultra-high vacuum conditions, the only potential chiral influence on the system was that of the STM tip itself. Previous studies have shown that is possible to functionalize scanning probe tips with both chiral and biological molecules[163-166], but usually regular metal STM tips are considered to be point sources of electrons.

Just as one's right and left hands should have the same dimensions, one would expect the R and S enantiomers of surface-bound BuSMe to have the same widths and heights. However, recent studies by this group have revealed that, in

any given experiment, either the R or S enantiomers would appear topographically higher.[153] While any particular tip yielded reproducible height differences between the enantiomers, alteration of the tip state led to a different height difference. Changes in the tip state were produced in the form of minor alterations via voltage pulses or surface indentations, or as major changes such as substitution of an entirely new tip.

In order to understand the origin of the symmetry breaking events, each different STM tip's intrinsic chirality (as measured by the height difference between R and S molecules) was correlated to the *ee* it produced after exciting precursor BuSMe molecules (Figure 9.2). The correlation between the tip's chirality and the *ee* of S produced after excitation of precursor molecules is shown in Figure 9.3. This graph demonstrates that STM tips that image the S enantiomers as topographically higher also produce larger *ee*'s of the S enantiomer. This data reveals an interesting new mechanism of chirality transfer by which the very subtle chirality in the geometric arrangement of the last few atoms at the end of a scanning probe tip can be imparted to prochiral molecules in a coherent manner.

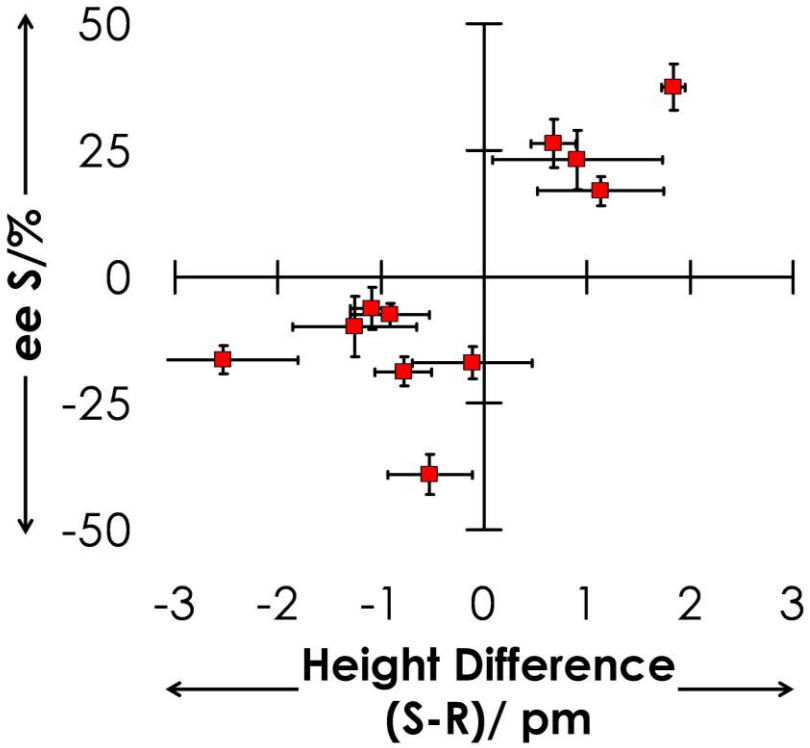

Figure 9.3: Origin of symmetry breaking. Graph relating the *ee* of the S molecules produced from electrical excitation of prochiral BuSMe on achiral Cu(111) to the "chirality" of the tip used for excitation. The height difference of the two enantiomers (R and S) serves as the metric for each STM tip's chirality.

To further interrogate the mechanism of this chirality transfer we monitored the *ee* when the direction of electron flow during the excitation process was reversed, making sure that the STM tip state had not changed between experiments. These experiments revealed that both positive and negative tip voltages gave *ee*'s of the same magnitude (25±5 % of enantiomer S). This result rules out both an electric field effect and a mechanism involving spin polarization of the tunneling current in the symmetry breaking process, as these mechanisms would result in the opposite enantiomer being favoured upon

reversal of the electron flow[157,160]. The independence of the *ee* on the direction of electron flow suggests that the role of the electrons is to supply the energy required for the precursor molecule to transition to its preferred adsorption site and that the geometric chirality of the tip imposes different kinetic barriers for chirality transfer into these two enantiomers.

A related effect has been observed for electron-induced dissociation of chiral molecules adsorbed on chiral Cu(643) metal surfaces in which the interaction strength of the molecule bonded directly to a chiral metallic surface site determines the lifetime of the excited state and hence the enantiospecific dissociation probability[167]. Our previous work has shown that the C-H stretch mode in thioethers has the highest cross-section for excitation by tunneling electrons (>375 meV) which suggests that the steep rise in the excitation probability of the precursor molecule >350 meV in this work occurs via the same pathway[90]. Two recent studies have reported that various motions of surface-bound chiral molecules could be excited by tunneling electrons in an analogous manner by which tunneling electrons excite high energy vibrations that then redistribute energy into rotation, translation and chirality inversion events[67,68].

9.4 Conclusions

Being able to measure a "degree of chirality" and quantify its transfer from one species to the next is crucial for advancing the understanding of the transfer of chirality that is at the heart of chiral separations, amplification, and

symmetry breaking processes[128,156-158,168]. We have observed *ee*'s of up to 39±5 %, higher than any ever reported as resulting from circularly polarized light or spin-polarized electron-induced processes[157-161,167]. We suggest that this system will open up new possibilities to interrogate the coupling of photons, electrons and combinations of physical fields to achiral starting systems and allow the mechanism of chirality transfer to be studied in a controllable manner. While we show in this paper that STM tips can have a dramatic symmetry breaking effect, once the molecules are in their equilibrium sites they are very stable with respect to further changes in chirality and can even be moved laterally between different adsorption sites while retaining their chirality. Therefore, by exposing prochiral starting materials to external chiral influences with the STM tip withdrawn, and then measuring resultant *ee*'s in situ, analogs of this system will allow symmetry breaking experiments to be performed in very well defined environments in which *ee*'s can be determined locally.

Chapter 10

Future Directions

Future studies will need to focus on coupling rotating molecules such as these to other machine parts. Just as macroscopic machines are often made up of many individual parts, it is unlikely that a single rotating motor would be sufficient to create a useful nanomachine. Initial studies may focus on coupling between just the rotating molecules. By creating arrays of rotors, it would be possible to study the coupling between molecules. When one molecule is forced to rotate, it would be possible to see how this affects its neighboring molecules. If the molecules were sufficiently static before rotation was induced, then it would be possible to measure the decay length from one molecule to its neighbors. Further studies could aim to couple rotating parts to other nanomachine parts, e.g. linear motors. Rotors in this case could act as a switch to set off a chain reaction between other parts in the machine.

Other fundamental studies could include rotors on {100} surfaces. All work described here was performed on {111} surfaces; a different surface facet would provide a different rotational barrier. Presumably if the rotational barrier was higher (and thus minimal rotational events were coming from thermal energy) then more rotational events would be occurring through the directional, electrically-driven channel. Other possibilities for increasing the surface-molecule bond strength could include changing the anchor bond by employing

different elements on either end of the bond (the central atom within the molecule, or the surface composition). Alloys also change the adsorption strength of incoming adsorbates by altering the electronic properties of the constituent elements in the surface. This may provide a stronger bond, which again could possibly lead to a higher degree of directionality for the rotating molecules.

An experiment based on a single-molecule version of the "Maxwell's Demon" thought experiment may provide an opportunity for a high degree of directionality. This experiment would require writing a programming code for the scanning software used for the STM. This code, used while taking a *I* vs. *t* curve, could bias the directionality by changing one key condition of the curve when the rotor changed position with respect to the tip. The most likely condition to change with this program would be the voltage set for the curve. In this way, for example, when the rotor switched to the highest current state (corresponding to the position of the rotor closest to the STM tip) the voltage used for the curves would be changed to a lower condition. Then when the rotor switched to a lower current state, the voltage would again be increased. Any inequality in curve taking such as this has been predicted to break the symmetry between neighboring current states, and create the ratchet potential needed for highly directional motion.

References

(1) Bray, D. *Cell Movements: from molecules to motility*, 2nd ed.; Garland Publishing: New York, 2001.

(2) Howard, J. *Mechanics of Motor Proteins and the Cytoskeleton*; Sinauer Associates: Sunderland, MA, 2001.

(3) Lodish, H. Z., S.L.; Matsudaira, P.; Baltimore, D.; Darnell, J. *Molecular Cell Biology*, 4th ed.; W.H. Freeman and Company: New York, 2000.

(4) Schliwa, M.; Woehlke, G. *Nature* **2003**, *422*, 759.

(5) Shirai, Y.; Morin, J. F.; Sasaki, T.; Guerrero, J. M.; Tour, J. M. *Chem. Soc. Rev.* **2006**, *35*, 1043.

(6) van Delden, R. A.*et al. Nature* **2005**, *437*, 1337.

(7) Hernandez, J. V.; Kay, E. R.; Leigh, D. A. *Science* **2004**, *306*, 1532.

(8) Kelly, T. R.; Silva, R. A.; De Silva, H.; Jasmin, S.; Zhao, Y. J. *J. Am. Chem. Soc.* **2000**, *122*, 6935.

(9) Koumura, N.; Zijlstra, R. W. J.; van Delden, R. A.; Harada, N.; Feringa, B. L. *Nature* **1999**, *401*, 152.

(10) Leigh, D. A.; Wong, J. K. Y.; Dehez, F.; Zerbetto, F. *Nature* **2003**, *424*, 174.

(11) Fendrich, M.; Wagner, T.; Stohr, M.; Moller, R. *Phys. Rev. B* **2006**, *73*, 115433.

(12) Gao, L.*et al. Phys. Rev. Lett.* **2008**, *101*, 197209.

(13) Gimzewski, J. K.*et al. Science* **1998**, *281*, 531.

(14) Hou, S. M.; Sagara, T.; Xu, D. C.; Kelly, T. R.; Ganz, E. *Nanotechnol.* **2003**, *14*, 566.

(15) Magnera, T. F.; Michl, J. Altitudinal surface-mounted molecular rotors. In *Molecular Machines*, 2005; Vol. 262; pp 63.

(16) Stohr, M.; Wagner, T.; Gabriel, M.; Weyers, B.; Moller, R. *Phys. Rev. B* **2002**, *65*, 33404.

(17) Takami, T.*et al. J. Phys. Chem. C* **2007**, *111*, 2077.

(18) Vaughan, O. P. H.; Williams, F. J.; Bampos, N.; Lambert, R. M. *Angew. Chem. Int. Ed.* **2006**, *45*, 3779.

(19) Ye, T.; Takami, T.; Wang, R. M.; Jiang, J. Z.; Weiss, P. S. *J. Am. Chem. Soc.* **2006**, *128*, 10984.

(20) Alvey, M. D.; Yates, J. T.; Uram, K. J. *J. Chem. Phys.* **1987**, *87*, 7221.

(21) Stipe, B. C.; Rezaei, M. A.; Ho, W. *Science* **1998**, *279*, 1907.

(22) Horinek, D.; Michl, J. *PNAS* **2005**, *102*, 14175.

(23) Hersam, M. C.; Guisinger, N. P.; Lyding, J. W. *J. Vac. Sci. Technol. A* **2000**, *18*, 1349.

(24) Wahl, M.; Stohr, M.; Spillmann, H.; Jung, T. A.; Gade, L. H. *Chem. Commun.* **2007**, *13*, 1349.

(25) Wintjes, N.*et al. Angew. Chem. Int. Ed.* **2007**, *46*, 4089.
(26) Dunphy, J. C.*et al. Phys. Rev. B* **1998**, *81*, 1263.
(27) Matsumoto, J. C.; Kim, Y.; Okawa, T.; Sainoo, Y.; Kawai, M. *Surf. Sci.* **2005**, *587*, 19.
(28) Sainoo, Y.; Kim, Y.; Komeda, T.; Kawai, M.; Shigekawa, H. *Surf. Sci.* **2003**, *536*, L403.
(29) Sainoo, Y.*et al. Phys. Rev. Lett.* **2005**, *95*, 2461021.
(30) Kottas, G. S.; Clarke, L. I.; Horinek, D.; Michl, J. *Chem. Rev.* **2005**, *105*, 1281.
(31) Clarke, L. I.*et al. Nanotechnol.* **2002**, *13*, 533.
(32) Wang, B.*et al. Nanotechnol.* **2004**, *15*, 324.
(33) Zheng, X. L.*et al. J. Am. Chem. Soc.* **2004**, *126*, 4540.
(34) Rao, B. V.; Kwon, K. Y.; Liu, A. W.; Bartels, L. *J. Chem. Phys.* **2003**, *119*, 10879.
(35) Rao, B. V.; Kwon, K. Y.; Liu, A. W.; Bartels, L. *Proc. Natl. Acad. Sci.* **2004**, *101*, 17920.
(36) Maksymovych, P.; Sorescu, D. C.; Dougherty, D.; Yates, J. T. *J. Phys. Chem. B* **2005**, *109*, 22463.
(37) Baber, A. E.; Tierney, H. L.; Sykes, C. H. *ACS Nano* **2008**, *2*, 2385.
(38) Bellisario, D. O.; Baber, A. E.; Tierney, H. L.; Sykes, E. C. H. *J. Phys. Chem. C* **2009**, *113*, 5895.
(39) Jensen, S. C.; Baber, A. E.; Tierney, H. L.; Sykes, E. C. H. *ACS Nano* **2007**, *1*, 423.
(40) Jensen, S. C.; Baber, A. E.; Tierney, H. L.; Sykes, E. C. H. *ACS Nano* **2007**, *1*, 22.
(41) Noh, J.; Murase, T.; Nakajima, K.; Lee, H.; Hara, M. *J. Phys. Chem. B* **2000**, *104*, 7411.
(42) Troughton, E. B.*et al. Langmuir* **1988**, *4*, 365.
(43) Weidner, T.*et al. J. Phys. Chem. C* **2009**, *113*, 19609.
(44) Liu, W.*et al. J. Am. Chem. Soc.* **2008**, *130*, 1274.
(45) Stuart, D. A.*et al. Anal. Chem.* **2006**, *78*, 7211.
(46) Dameron, A. A.*et al. Nano Lett.* **2005**, *5*, 1834.
(47) Love, J. C.; Estroff, L. A.; Kriebel, J. K.; Nuzzo, R. G.; Whitesides, G. M. *Chem. Rev.* **2005**, *105*, 1103.
(48) Donhauser, Z. J.*et al. Science* **2001**, *292*, 2303.
(49) Xia, Y. N.; Whitesides, G. M. *Angew. Chem.-Int. Edit.* **1998**, *37*, 551.
(50) Li, X. M.*et al. J. Mater. Chem.* **2001**, *11*, 1919.
(51) Maye, M. M.*et al. J. Am. Chem. Soc.* **2005**, *127*, 1519.
(52) Shelley, E. J.*et al. Langmuir* **2002**, *18*, 1791.
(53) Lavrich, D. J.; Wetterer, S. M.; Bernasek, S. L.; Scoles, G. *J. Phys. Chem. B* **1998**, *102*, 3456.
(54) Backer, T.; Hovel, H.; Tschudy, M.; Reihl, B. *Appl. Phys. A* **1998**, *66*, S27.

(55) Horinek, D.; Michl, J. *J. Am. Chem. Soc.* **2003**, *125*, 11900.
(56) Vacek, J.; Michl, J. *Adv. Funct. Mater.* **2007**, *17*, 730.
(57) Akimov, A. V.; Nemukhin, A. V.; Moskovsky, A. A.; Kolomeisky, A. B.; Tour, J. M. *J. Chem. Theory Comput.* **2008**, *4*, 652.
(58) Okumura, H.; Itoh, S. G.; Okamoto, Y. J. *J. Chem. Phys.* **2007**, *126*, 084103.
(59) Dullweber, A.; Leimkuhler, B.; McLahlan, F. *J. Chem. Phys.* **1997**, *107*, 5840.
(60) Rappe, A. K.; Casewit, C. J.; Colwell, K. S.; Goddard III, W. A.; Skiff, W. M. *J. Am. Chem. Soc.* **1992**, *114*, 10024.
(61) Mahaffy, R.; Bhatia, R.; Garrison, B. J. *J. Phys. Chem. B* **1997**, *101*, 771.
(62) Tierney, H. L.; Baber, A. E.; Sykes, E. C. H.; Akimov, A.; Kolomeisky, A. B. *J. Phys. Chem. C* **2009**, *113*, 10913.
(63) Komeda, T.; Kim, Y.; Kawai, M.; Persson, B. N. J.; Ueba, H. *Science* **2002**, *295*, 2055.
(64) Ohara, M.; Kim, Y.; Yanagisawa, S.; Morikawa, Y.; Kawai, M. *Phys. Rev. Lett.* **2008**, *100*.
(65) Pascual, J. I.; Lorente, N.; Song, Z.; Conrad, H.; Rust, H.-P. *Nature* **2003**, *423*, 525.
(66) Stipe, B. C.; Rezaei, M. A.; Ho, W. *Phys. Rev. Lett.* **1998**, *81*, 1263.
(67) Parschau, M.; Passerone, D.; Rieder, K. H.; Hug, H. J.; Ernst, K. H. *Angew. Chem. Int. Ed.* **2009**, *48*, 4065.
(68) Simic-Milosevic, V.; Meyer, J.; Morgenstern, K. *Angew. Chem. Int. Ed.* **2009**, *48*, 4061
(69) Lauhon, L. J.; Ho, W. *Phys. Rev. Lett.* **2000**, *84*, 1527.
(70) Sainoo, Y.; Kim, Y.; Komeda, T.; Kawai, M. *J. Chem. Phys.* **2004**, *120*, 7249.
(71) Stipe, B. C.; Rezaei, M. A.; Ho, W. *Science* **1998**, *280*, 1732.
(72) Lauhon, L. J.; Ho, W. *J. Phys. Chem. A* **2000**, *104*, 2463.
(73) Wong, K. L.; Kwon, K. Y.; Bartels, L. *Appl. Phys. Lett.* **2006**, *88*.
(74) Watson, D. J.*et al. J. Am. Chem. Soc.* **2009**, *131*, 14584.
(75) Illa, O.; Arshad, M.; Ros, A.; McGarrigle, E. M.; Aggarwal, V. K. *J. Am. Chem. Soc.* **2010**, *132*, 1828.
(76) Peterle, T.; Ringler, P.; Mayor, M. *Adv. Funct. Mater.* **2009**, *19*, 3497.
(77) Kautz, N. A.; Kandel, S. A. *J. Am. Chem. Soc.* **2008**, *130*, 6908.
(78) Maksymovych, P.; Yates, J. T. *J. Am. Chem. Soc.* **2008**, *130*, 7518.
(79) Nenchev, G.; Diaconescu, B.; Hagelberg, F.; Pohl, K. *Phys. Rev. B* **2009**, *80*.
(80) Stepanow, S.*et al. Angew. Chem.-Int. Edit.* **2007**, *46*, 710.
(81) Makoudi, Y.*et al. Surf. Sci.* **2008**, *602*, 2719.
(82) Weigelt, S.*et al. Nat. Mater.* **2006**, *5*, 112.

(83) Fasel, R.; Parschau, M.; Ernst, K. H. *Angew. Chem.-Int. Edit.* **2003**, *42*, 5178.
(84) Bohringer, M.*et al. Phys. Rev. Lett.* **1999**, *83*, 324.
(85) Rao, B. V.; Kwon, K. Y.; Zhang, J.; Liu, A. W.; Bartels, L. *Langmuir* **2004**, *20*, 4406.
(86) Bengtsson, L. *Phys. Rev. B* **1999**, *59*, 12301.
(87) Neugebauer, J.; Scheffler, M. *Phys. Rev. B* **1992**, *46*, 16067.
(88) Henkelman, G.; Jonsson, H. *J. Chem. Phys.* **2000**, *113*, 9978.
(89) Henkelman, G.; Uberuaga, B. P.; Jonsson, H. *J. Chem. Phys.* **2000**, *113*, 9901.
(90) Tierney, H. L.*et al. Chem. Eur. J.* **2009**, *15*, 9678.
(91) Tierney, H. L.; Calderon, C. E.; Baber, A. E.; Sykes, E. C. H.; Wang, F. *J. Phys. Chem. C* **2010**, *114*, 3152.
(92) Henkelman, G.; Arnaldsson, A.; Jonsson, H. *Comp. Mater. Sci.* **2006**, *36*, 354.
(93) Sanville, E.; Kenny, S. D.; Smith, R.; Henkelman, G. *J. Comput. Chem.* **2007**, *28*, 899.
(94) Tang, W.; Sanville, E.; Henkelman, G. *J. Phys.-Condes. Matter* **2009**, *21*, 084204.
(95) Briner, B. G.; Doering, M.; Rust, H. P.; Bradshaw, A. M. *Science* **1997**, *278*, 257.
(96) Chung, C. H.; Jung, W. J.; Lyo, I. W. *Phys. Rev. Lett.* **2006**, *97*, 116102.
(97) Jewell, A. D.*et al. J. Phys.-Condes. Matter* **2010**, *22*, 264006.
(98) Sholl, D. S.; Steckel, J. A. *Density Functional Theory: A Practical Introduction*; John Wiley & Sons: Hoboken, NJ, 2009.
(99) Newton, T. A.; Huang, Y. C.; Lepak, L. A.; Hines, M. A. *J. Chem. Phys.* **1999**, *111*, 9125.
(100) Hwang, I. S.; Lo, R. L.; Tsong, T. T. *Surf. Sci.* **1998**, *399*, 173.
(101) Tysoe, W. T.; Ormerod, R. M.; Lambert, R. M.; Zgrablich, G.; Ramirezcuesta, A. *J. Phys. Chem.* **1993**, *97*, 3365.
(102) Miwa, J. A.*et al. J. Am. Chem. Soc.* **2006**, *128*, 3164.
(103) Maraghechi, P.; Horn, S. A.; Patitsas, S. N. *Surf. Sci.* **2007**, *601*, L1.
(104) Suzuki, S.*et al. Catal. Lett.* **1998**, *50*, 117.
(105) Stranick, S. J.; Kamna, M. M.; Weiss, P. S. *Science* **1994**, *266*, 99.
(106) Tsukahara, N.; Mukai, K.; Yamashita, Y.; Yoshinobu, J. *J. Chem. Phys.* **2008**, *128*.
(107) Yoshinobu, J.; Tsukahara, N.; Yasui, F.; Mukai, K.; Yamashita, Y. *Phys. Rev. Lett.* **2003**, *90*.
(108) Albers, B. J.*et al. Nat. Nanotechnol.* **2009**, *4*, 307.
(109) Schwarz, A.; Allers, W.; Schwarz, U. D.; Wiesendanger, R. *Phys. Rev. B* **2000**, *61*, 2837.
(110) Ternes, M.; Lutz, C. P.; Hirjibehedin, C. F.; Giessibl, F. J.; Heinrich, A. J. *Science* **2008**, *319*, 1066.

(111) Kwon, K. Y.*et al. Phys. Rev. Lett.* **2005**, *95*.
(112) Grunze, M.; Kreuze, H. J. *Kinetics of Interface Reactions*; Springer: Berlin, 1987.
(113) Stipe, B. C.; Rezaei, M. A.; Ho, W. *J. Chem. Phys.* **1997**, *107*, 6443.
(114) Brown, D. E.; Moffatt, D. J.; Wolkow, R. A. *Science* **1998**, *279*, 542.
(115) Sautet, P.; Bocquet, M. L. *Surf. Sci.* **1994**, *304*, L445.
(116) Weiss, P. S.; Eigler, D. M. *Phys. Rev. Lett.* **1993**, *71*, 3139.
(117) Brown, D. E.; Sholl, D. S.; Skodje, R. T.; George, S. M. *Chem. Phys.* **1995**, *201*, 273.
(118) Tsong, T. T.; Fu, T. Y. *Appl. Surf. Sci.* **1997**, *121*, 34.
(119) Tierney, H. L.*et al. J. Phys. Chem. C* **2010**, In Press.
(120) Sykes, E. C. H.; Mantooth, B. A.; Han, P.; Donhauser, Z. J.; Weiss, P. S. *J. Am. Chem. Soc.* **2005**, *127*, 7255.
(121) Seebauer, E. G.; Allen, C. E. *Prog. Surf. Sci.* **1995**, *49*, 265.
(122) Nilekar, A. U.; Greeley, J.; Mavrikakis, M. *Angew. Chem.-Int. Edit.* **2006**, *45*, 7046.
(123) Pilling, M. J.; Seakins, P. W. *Reaction Kinetics*; Oxford University Press: Oxford, UK, 1995.
(124) Bohringer, M.; Morgenstern, K.; Schneider, W. D.; Berndt, R. *Angew. Chem.-Int. Edit.* **1999**, *38*, 821.
(125) Chen, Q.; Richardson, N. V. *Nat. Mater.* **2003**, *2*, 324.
(126) De Feyter, S.*et al. Angew. Chem. Int. Ed.* **1998**, *37*, 1223.
(127) Fang, H. B.; Giancarlo, L. C.; Flynn, G. W. *J. Phys. Chem. B* **1998**, *102*, 7311.
(128) Fasel, R.; Parschau, M.; Ernst, K. H. *Nature* **2006**, *439*, 449.
(129) Greber, T.; Sljivancanin, Z.; Schillinger, R.; Wider, J.; Hammer, B. *Phys. Rev. Lett.* **2006**, *96*, 056103.
(130) Kuhnle, A.; Linderoth, T. R.; Hammer, B.; Besenbacher, F. *Nature* **2002**, *415*, 891.
(131) Kuzmenko, I.; Weissbuch, I.; Gurovich, E.; Leiserowitz, L.; Lahav, M. *Chirality* **1998**, *10*, 415.
(132) Lingenfelder, M.*et al. Angew. Chem.-Int. Edit.* **2007**, *46*, 4492.
(133) Lopinski, G. P.; Moffatt, D. J.; Wayner, D. D. M.; Wolkow, R. A. *Nature* **1998**, *392*, 909.
(134) Lorenzo, M. O.; Baddeley, C. J.; Muryn, C.; Raval, R. *Nature* **2000**, *404*, 376.
(135) Marschall, M.*et al. ChemPhysChem* **2010**, *11*, 1446.
(136) Mulligan, A.*et al. Angew. Chem.-Int. Edit.* **2005**, *44*, 1830.
(137) Xu, H.*et al. ACS Nano* **2009**, *3*, 1016.
(138) Busalla, A.; Blum, K.; Thompson, D. G. *Phys. Rev. Lett.* **1999**, *83*, 1562.
(139) Smith, I. M.; Thompson, D. G.; Blum, K. *J. Phys. B-At. Mol. Opt. Phys.* **1998**, *31*, 4029.

(140) Yeganeh, S.; Ratner, M. A.; Medina, E.; Mujica, V. *J. Chem. Phys.* **2009**, *131*.
(141) Haq, S.; Liu, N.; Humblot, V.; Jansen, A. P. J.; Raval, R. *Nat. Chem.* **2009**, *1*, 409.
(142) Gellman, A. J. *ACS Nano* **2010**, *4*, 5.
(143) Attard, G. A. *J. Phys. Chem. B* **2001**, *105*, 3158.
(144) Garzon, I. L.*et al. Eur. Phys. J. D* **2003**, *24*, 105.
(145) Lauhon, L. J.; Ho, W. *Rev. Sci. Instrum.* **2001**, *72*, 216.
(146) Balzani, V.; Credi, A.; Venturi, M. *Molecular Devices and Machines: A Journey into the Nanoworld*; Wiley-VCH: Weinheim, Germany, 2004.
(147) Kay, E. R.; Leigh, D. A.; Zerbetto, F. *Angew. Chem. Int. Ed.* **2007**, *46*, 72.
(148) von Delius, M.; Geertsema, E. M.; Leigh, D. A. *Nat. Chem.* **2010**, *2*, 96.
(149) Klok, M.*et al. J. Am. Chem. Soc.* **2008**, *130*, 10484.
(150) Wang, W.*et al. ACS Nano* **2010**, *4*, 4929.
(151) Zhong, D. Y.*et al. Nano Lett.* **2009**, *9*, 4387.
(152) Cahn, V.; Ingold, C. K.; Prelog, V. *Angew. Chem. Int. Ed.* **1966**, *5*, 385.
(153) Tierney, H. L.; Murphy, C. J.; Sykes, E. C. H. *Phys. Rev. Lett.* **2010**, *Submitted*.
(154) Booth, T. D.; Wahnon, D.; Wainer, I. W. *Chirality* **1997**, *9*, 96.
(155) Pasteur, L. *Ann. Chim. Phys.* **1848**, *24*, 442.
(156) Ortega-Lorenzo, M.; Baddeley, C. J.; Muryn, C.; Raval, R. *Nature* **2000**, *404*, 376.
(157) Avalos, M.*et al. Chem. Rev.* **1998**, *98*, 2391.
(158) Inoue, Y. *Chem. Rev.* **1992**, *92*, 741.
(159) Bonner, W. A.; Bean, B. D. *Origins Life Evol. Biosphere* **2000**, *30*, 513.
(160) Rosenberg, R. A.; Abu Haija, M.; Ryan, P. J. *Phys. Rev. Lett.* **2008**, *101*.
(161) Rikken, G.; Raupach, E. *Nature* **2000**, *405*, 932.
(162) Tierney, H. L.; Jewell, A. D.; Baber, A. E.; Iski, E. V.; Sykes, E. C. H. *Langmuir* **2010**, *26*, 15350.
(163) Chang, S.*et al. Nat. Nanotechnol.* **2009**, *4*, 297.
(164) McKendry, R.; Theoclitou, M. E.; Rayment, T.; Abell, C. *Nature* **1998**, *391*, 566.
(165) Nishino, T.; Umezawa, Y. *Anal. Chem.* **2008**, *80*, 6968.
(166) Lo, Y. S.*et al. Langmuir* **1999**, *15*, 1373.
(167) Fleming, C.; King, M.; Kadodwala, M. *J. Phys. Chem. C* **2008**, *112*, 18299.
(168) Weissbuch, I.; Leiserowitz, L.; Lahav, M. Stochastic "Mirror symmetry breaking" via self-assembly, reactivity and amplification of chirality: Relevance to abiotic conditions. In *Prebiotic Chemistry: From Simple Amphiphiles to Protocell Models*, 2005; Vol. 259; pp 123.